JACS
JOURNAL OF THE AMERICAN CHEMICAL SOCIETY
Article
pubs.acs.org/JACS

Dispersion Forces and Counterintuitive Steric Effects in Main Group Molecules: Heavier Group 14 (Si–Pb) Dichalcogenolate Carbene Analogues with Sub-90° Interligand Bond Angles

Brian D. Rekken,[†] Thomas M. Brown,[†] James C. Fettinger,[†] Felicitas Lips,[†] Heikki M. Tuononen,[§] Rolfe H. Herber,[‡] and Philip P. Power*[,†]

[†]Department of Chemistry, University of California, Davis, One Shields Avenue, Davis, California, 95616, United States
[‡]Racah Institute of Physics, Hebrew University of Jerusalem, 91904, Jerusalem, Israel
[§]Department of Chemistry, University of Jyväskylä, P.O. Box 35, FI-40014 Jyväskylä, Finland

Supporting Information

ABSTRACT: The synthesis and spectroscopic and structural characterization of an extensive series of acyclic, monomeric tetrylene dichalcogenolates of formula $M(ChAr)_2$ (M = Si, Ge, Sn, Pb; Ch = O, S, or Se; Ar = bulky *m*-terphenyl ligand, including two new acyclic silylenes) are described. They were found to possess several unusual features—the most notable of which is their strong tendency to display acute interligand, Ch–M–Ch, bond angles that are often well below 90°. Furthermore, and contrary to normal steric expectations, the interligand angles were found to become narrower as the size of the ligand was increased. Experimental and structural data in conjunction with high-level DFT calculations, including corrections for dispersion effects, led to the conclusion that dispersion forces play an important role in stabilizing their acute interligand angles.

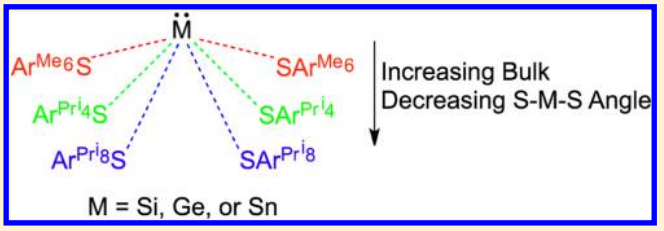

INTRODUCTION

The use of sterically crowding ligands to influence chemical reactivity, to protect reactive sites, and to stabilize molecules with unusual bonding or low coordination numbers is a well-established and powerful technique in molecular chemistry. Such ligands have been crucial for the synthesis of numerous new molecular classes throughout the periodic table.[1] For example, a considerable portion of modern main group chemistry is sustained by their employment in the isolation of compounds with previously unknown oxidation states or bonding, where stability is achieved by blocking decomposition routes that often involve disproportionation or polymerization reactions.[2] The crowded environments produced by the ligands introduce some degree of steric strain due to overlapping electron clouds. The presence of strain is usually manifested in the distortion of structural parameters and may result in bond lengthening and the widening of interligand angles to reduce the congestion.[3] The distortions can, in extreme instances, lead to bond cleavage or dissociation[4] or molecular rearrangement.[5] In such cases, the cause and effect relationship between the strain and geometrical distortion appears to be intuitively obvious. However, in this paper we shall describe the synthesis and characterization of a series of compounds (the dichalcogenolates of divalent group 14 elements) where such trends are apparently reversed, so that increasing the size of the ligand leads to a decrease, rather than an increase, in the interligand angles.

The neutral bis-chalcogenolate derivatives of the heavier group 14 elements form part of a wider class of stable, monomeric species (metallylenes) of formula MR_2 (M = Si, Ge, Sn, or Pb; R = alkyl, aryl, silyl, amido, phosphido, alkoxo, etc.) which are analogous to carbenes and for which more than 250 stable examples are currently known.[6] They possess V-shaped geometries with interligand angles that are usually well below 120°, but generally >90°. The angles decrease with increasing atomic number of the group 14 element and increasing electronegativity of the ligand in accordance with Bent's rule.[7] In isolated cases, interligand angles below the expected lower limit of 90° (on the basis of the 90° angle between the valence p-orbitals) have been observed, as in $Sn(OC_6H_2\text{-}2,6\text{-}Bu^t_2\text{-}4\text{-}Me)_2$ (O–Sn–O = 88.8(2)°),[8] $Sn(SMes^*)_2$ ($Mes^* = C_6H_2\text{-}2,4,6\text{-}Bu^t_3$; S–Sn–S = 85.4(1)°),[9] or the bis primary amides $M\{N(H)Ar^{Me_6}\}_2$ (N–M–N = 88.6(2)°, Ge; 87.07(8)°, Sn; 87.47(9)°, Pb; $Ar^{Me_6} = C_6H_3\text{-}2,6(C_6H_2\text{-}2,4,6\text{-}Me_3)_2$).[10] Recently, we demonstrated that the terphenyl chalcogenolate ligands, $\text{-}OAr^{Pr^i_4}$ and $\text{-}SAr^{Pr^i_4}$ ($Ar^{Pr^i_4} = C_6H_3\text{-}2,6\text{-}(C_6H_3\text{-}2,6\text{-}Pr^i_2)_2$) produced very different interligand angles in their divalent lead derivatives $Pb(OAr^{Pr^i_4})_2$ (O–Pb–O = 99(1)° average value) and $Pb(SAr^{Pr^i_4})_2$ (S–Pb–S = 77.21(4)°).[11] The latter angle was the narrowest reported for a group 14 element metallylene derivative. We also showed that the use of the somewhat less crowding chalcogenolate ligand $-SAr^{Me_6}$ ($Ar^{Me_6} = C_6H_3\text{-}2,6\text{-}(C_6H_2\text{-}2,4,6\text{-}Me_3)_2$) stabilized an acyclic silylene, $Si(SAr^{Me_6})_2$,[12]

Received: April 16, 2013

   dx.doi.org/10.1021/ja403802a | J. Am. Chem. Soc. XXXX, XXX, XXX–XXX

(reported essentially simultaneously to the acyclic silylene, Si{N(SiMe$_3$)(Dipp)}{BN(Dipp)CHCHN(Dipp)} (Dipp = C$_6$H$_3$-2,6-Pr$^i_2$) by Aldridge and Jones)[13] which possesses a relatively narrow interligand angle 90.52(2)°.[1,14] These unusual angular variations suggested that a more extensive study on a larger range of compounds was warranted to explain their origin. We now describe our experimental and computational studies of an extensive series (a total of 20 compounds, of which 14 are newly described, including 2 new acyclic silylenes) of low-valent dichalocogenolate, ChAr (Ch = O, S, Se; Ar = terphenyl), derivatives of Si, Ge, Sn, and Pb. The data show that interligand angles as low as 73.09(2)° can be obtained and that the Ch−M−Ch angle depends on a variety of factors, including steric interactions across the 2-fold axis bisecting the ChMCh bond. DFT calculations employing a correction for dispersion effects provide further insight to the bonding and show that attractive dispersion forces between the alkyl substituents of the terphenyl ligands play an important role in narrowing the interligand angles. All of the compounds are stabilized by chalcogenolate ligands bearing the terphenyl substituents illustrated in Figure 1.

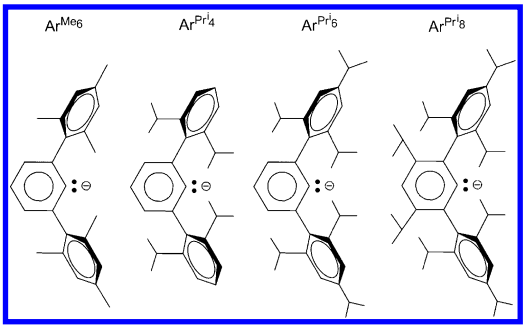

Figure 1. The terphenyl group substituent anions display increasing bulk moving from left to right. The *ipso* carbon is bonded to O, S, or Se.

EXPERIMENTAL SECTION

General Procedures. All manipulations were performed with the use of modified Schlenk techniques under an N_2 atmosphere or in a Vacuum Atmospheres drybox under N_2 except the magnesium reductions, which were performed under argon. Solvents were distilled over a potassium mirror and degassed immediately prior to use via freeze−pump−thaw cycles. Unless otherwise noted, all chemicals were obtained from commercial sources and used without further purification. Rieke's magnesium[15,16] and the thiols Ar^{Me_6}SH, Ar$^{Pr^i_4}$SH, and Ar$^{Pr^i_6}$SH as well as their alkali metal salts were prepared by literature procedures.[17] The thiol, Ar$^{Pr^i_8}$SH (see Supporting Information (SI), **30**), was prepared by reaction of Ar$^{Pr^i_8}$Li(OEt$_2$)[18] with sulfur employing the same synthetic procedure as that used for Ar$^{Pr^i_6}$SH.[17c] The MSeAr$^{Pr^i_4}$ (M = Li, K) salts were prepared by addition of either LiBu^n or K metal to the air-stable triselenine, Se(SeAr$^{Pr^i_4}$)$_2$ (see SI).[19] ^{1}H NMR and ^{13}C NMR spectra were recorded on either a Varian 300, 400, or 600 MHz instrument and referenced internally to either protio benzene or trace silicon grease (δ = 0.29 in C$_6$D$_6$). ^{29}Si NMR spectra were acquired on a Varian 600 MHz (operating at 119.14 MHz) instrument referenced to an external standard of SiMe$_4$ (TMS) (δ = 0) in C$_6$D$_6$. ^{77}Se NMR spectra were acquired on a Varian 600 MHz (operating at 114.4 MHz) instrument and were externally referenced to a saturated solution of selenous acid in D$_2$O (δ = 1300). ^{119}Sn (223.63 MHz) and ^{207}Pb (125.53 MHz) NMR spectra were acquired on a Varian 600 MHz instrument and were referenced to SnBu$^n_4$ in C$_6$D$_6$ (δ = −11.7) or PbMe$_4$ in C$_6$D$_6$ (δ = 0). IR spectra were recorded as Nujol mulls between KBr or CsI plates on a Perkin-Elmer 1430 spectrophotometer. UV−vis spectra were recorded as dilute hexanes solutions in 3.5 mL quartz cuvettes using a HP 8452 diode-array spectrophotometer. Melting points were determined on a Meltemp II apparatus using glass capillaries sealed with vacuum grease and are uncorrected.

*Si(SAr$^{Pr^i_4}$)$_2$ (**2**).* Si(Br)$_2$(SAr$^{Pr^i_4}$)$_2$ (1.698 g, 1.62 mmol; see compound **27**, SI) in THF (45 mL) was added over 10 min to a chilled suspension of Rieke's magnesium (0.0493 g, 2.03 mmol), freshly prepared in 40 mL of THF, and sonicated with a catalytic amount of anthracene for 3 h. The solution became red and, after 30 min, was allowed to warm to ambient temperature and stirred for a further 5 days. All the volatile components were removed under reduced pressure, and ca. 60 mL of hexanes and ca. 12 mL of 1,4-dioxane were added. The resultant solution was stirred for 24 h and filtered to give a clear, red solution. All of the volatile components were removed under reduced pressure, and the residue was redissolved in hexanes (12 mL), which were concentrated to ca. 3 mL storage in a ca. −18 °C refrigerator. This afforded small yellow needles of **2** after 1 week. Yield: (0.243 g, 0.27 mmol, 16.9%); mp 203−207 °C. Calcd for C$_{60}$H$_{74}$S$_2$Si: C, 81.2; H, 8.41. Found: C, 80.4; H, 8.23. ^{1}H NMR (399.8 MHz, C$_6$D$_6$, 295 K): δ = 1.07 (d, 24H, *o*-CH(C*H*$_3$)$_2$, $^3J_{H,H}$ = 6.80 Hz), 1.19 (d, 24H, *o*-CH(C*H*$_3$)$_2$, $^3J_{H,H}$ = 7.20 Hz), 2.69 (m, 8H, *o*-C*H*(CH$_3$)$_2$, $^3J_{H,H}$ = 6.80 Hz), 6.97 (t, 2H, *p*-C$_6$H$_3$, $^3J_{H,H}$ = 6.80 Hz), 7.05 (d, 4H, *m*-C$_6$H$_3$, $^3J_{H,H}$ = 7.2 Hz), 7.10 (d, 8H, *m*-C$_6$H$_3$Pr$^i_2$, $^3J_{HH}$ = 6.80 Hz), 7.20 (t, 4H, *p*-C$_6$H$_3$Pr$^i_2$, $^3J_{HH}$ = 7.20 Hz); ^{13}C{^{1}H} NMR (100.5 MHz, C$_6$D$_6$, 296 K): δ =23.34 (*o*-CH(CH$_3$)$_2$), 25.39 (*o*-CH(CH$_3$)$_2$), 31.23 (*o*-CH(CH$_3$)$_2$), 123.55 (*m*-C$_6$H$_3$Pr$^i_2$), 125.41 (*p*-C$_6$H$_3$), 128.97 (*m*-C$_6$H$_3$), 129.78 (*o*-C$_6$H$_3$), 137.38 (*p*-C$_6$H$_3$Pr$^i_2$), 138.87 (*o*-C$_6$H$_3$Pr$^i_2$), 141.85 (*i*-C$_6$H$_2$Pr$^i_2$), 147.05 (*i*-C$_6$H$_3$Pr$^i_2$); ^{29}Si NMR (119.1 MHz, C$_6$D$_6$, 295 K): δ = 270.4; UV−vis: [λ, nm (ε, M^{-1}cm^{-1})] 405 (3700), 318 (7400), 290 (11 200). IR (cm^{-1}): The Si−S stretching band tentatively assigned to an absorption at 648 cm^{-1}. A small portion of the silylene (0.05 g) was mixed with the potassium thiolate, K$_2$(SAr$^{Pr^i_4}$)$_2$ (see SI) and dissolved in a mixture of 1,4-dioxane (ca. 2 mL) and hexanes (ca. 2 mL) and placed in a ca. 7 °C refrigerator to yield X-ray quality crystals of **2** after 3 days.

*Si(SAr$^{Pr^i_6}$)$_2$ (**3**).* Si(Br)$_2$(SAr$^{Pr^i_6}$)$_2$ (1.141 g, 0.94 mmol; see compound **28**, SI) in THF (45 mL) was added over 10 min to a chilled suspension of Rieke's magnesium (0.0285 g, 1.17 mmol), freshly prepared in 40 mL of THF, and sonicated with a catalytic amount of anthracene for 3 h. The solution became red and was allowed to warm to ambient temperature and stirred for a further 3 days. All the volatile components were removed under reduced pressure, and hexanes (ca. 65 mL) and 1,4-dioxane (ca. 8 mL) were added and stirred for 24 h. Filtration yielded a clear, red solution which was concentrated to ca. 8 mL and placed in a ca. 7 °C refrigerator. Small yellow crystalline blocks of **3** (0.201 g) were obtained and isolated after 3 days. The supernatant liquid was evaporated to dryness, and the yellow residue was redissolved in toluene (ca. 15 mL). The resultant solution was concentrated to ca. 8 mL under reduced pressure and placed in a ca. 7 °C refrigerator to yield X-ray quality yellow crystals of **3**. Yield: (0.422 g total weight, 0.40 mmol, 42.6%); mp: 254−257 °C. Calcd for C$_{72}$H$_{98}$S$_2$Si: C, 81.91; H, 9.36. Found: C, 81.01; H, 9.08. ^{1}H NMR (599.7 MHz, C$_6$D$_6$, 295 K): δ = 1.12 (d, 24H, *o*-CH(C*H*$_3$)$_2$, $^3J_{H,H}$ = 6.99 Hz), 1.25 (d, 24H, *o*-CH(C*H*$_3$)$_2$, $^3J_{H,H}$ = 6.99 Hz), 1.33 (d, 24H, *p*-CH(C*H*$_3$)$_2$, $^3J_{H,H}$ = 7.00 Hz), 2.75 (m, 8H, *o*-C*H*(CH$_3$)$_2$, $^3J_{H,H}$ = 6.99 Hz), 2.89 (m, 4H, *p*-C*H*(CH$_3$)$_2$, $^3J_{H,H}$ = 6.99 Hz), 6.93 (t, 2H, *p*-C$_6$H$_3$, $^3J_{H,H}$ = 7.63 Hz), 7.05 (d, 4H, *m*-C$_6$H$_3$, $^3J_{H,H}$ = 7.63 Hz), 7.12 (s, 8H, *m*-C$_6$H$_2$Pr$^i_3$); ^{13}C{^{1}H} NMR (C$_6$D$_6$, 150.8 MHz, 295 K): δ = 23.62 (*o*-CH(CH$_3$)$_2$), 24.50 (*o*-CH(CH$_3$)$_2$), 25.56 (*o*-CH(CH$_3$)$_2$), 31.28 (*p*-CH(CH$_3$)$_2$), 34.81 (*p*-CH(CH$_3$)$_2$), 121.48 (*p*-C$_6$H$_3$), 125.36 (*m*-C$_6$H$_2$Pr$^i_3$), 130.11 (*m*-C$_6$H$_3$), 136.87 (*o*-C$_6$H$_3$), 138.04 (*o*-C$_6$H$_2$Pr$^i_3$), 141.66 (*p*-C$_6$H$_2$Pr$^i_3$), 146.84 (*i*-C$_6$H$_2$Pr$^i_3$), 148.92 (*i*-C$_6$H$_3$); ^{29}Si NMR (119.1 MHz, C$_6$D$_6$, 295 K): δ = 270.9; UV−vis: [λ, nm (ε, M^{-1}cm^{-1})] 411 (4400), 331 (7500), 290 (10 500). IR (cm^{-1}): The Si−S stretching band was tentatively assigned to an absorption at 645 cm^{-1}.

*Ge(SAr$^{Pr^i_4}$)$_2$ (**5**).* A solution of LiSAr$^{Pr^i_4}$ (1.253 g, 2.87 mmol) in diethyl ether (60 mL) was added dropwise over 45 min to a diethyl ether slurry (5 mL) of GeCl$_2$(1,4-dioxane) (0.332 g, 1.43 mmol) cooled to ca. 0 °C. The solution became yellow, and after 30 min, was allowed to warm to

dx.doi.org/10.1021/ja403802a | J. Am. Chem. Soc. XXXX, XXX, XXX−XXX

ambient temperature and stirred for a further 12 h. All volatile components were removed under reduced pressure, and the residue was extracted with hexanes (50 mL) and filtered. The solution was concentrated to ca. 4 mL and cooled to −17 °C to give **5** as a microcrystalline, threadlike solid. A small amount of **5** (ca. 0.04 g) was dissolved in a concentrated THF solution and stored at −17 °C for 3 days to yield X-ray yellow quality crystals of **5**. Yield: (0.943 g, 1.01 mmol, 70.5%). mp 203−206 °C. ^{1}H NMR (399.8 MHz, C_6D_6, 294 K): δ = 1.07 (d, 24H, CH(C*H*)$_2$, $^3J_{HH}$ = 6.83 Hz), 1.20 (d, 24H, CH(C*H*)$_2$, $^3J_{HH}$ = 6.83 Hz), 2.72 (m, 8H, C*H*(CH)$_2$, $^3J_{HH}$ = 6.83 Hz), 6.94 (t, 2H, *p*-C_6H_3, $^3J_{HH}$ = 7.51 Hz), 7.04 (d, *m*-C_6H_3, 4H, $^3J_{HH}$ = 7.41 Hz), 7.10 (d, 8H, *m*-$C_6H_3Pr^i_2$, $^3J_{HH}$ = 7.41 Hz), 7.20 (t, 4H, *p*-$C_6H_3Pr^i_2$, $^3J_{HH}$ = 6.84 Hz); ^{13}C{^{1}H} NMR (100.5 MHz, C_6D_6, 296 K): δ = 23.46 (*o*-CH(*C*H$_3$)$_2$), 25.23 (*o*-CH(*C*H$_3$)$_2$), 31.16 (*o*-C*H*(CH$_3$)$_2$), 123.81 (*m*-$C_6H_2Pr^i_3$), 124.64 (*p*-C_6H_3), 128.89 (*m*-C_6H_3), 129.44 (*o*-C_6H_3), 139.39 (*p*-$C_6H_2Pr^i_2$), 139.97 (*o*-$C_6H_2Pr^i_2$), 141.12 (*i*-$C_6H_2Pr^i_2$), 147.12 (*i*-C_6H_3); UV−vis: [λ, nm (ε, M^{-1}cm^{-1})] 410 (3100), 330 (3600), 278 (5600).

*Ge(SAr$^{Pr^i_6}$)$_2$ (**6**).* A flask containing LiSAr$^{Pr^i_6}$ (1.518 g, 2.91 mmol) and $GeCl_2$(1,4-dioxane) (0.338 g, 1.43 mmol), was cooled to ca. −78 °C. Diethyl ether (65 mL) was added slowly over 20 min to afford a solution which, after 2 h, was allowed to warm to ambient temperature, after which time stirring was continued for 24 h. All volatile components were removed under reduced pressure and the residue was extracted with toluene (40 mL) and filtered. The solution was concentrated to ca. 4 mL and cooled to ca. −17 °C to give **6** as a yellow microcrystalline solid. Crystals of **6** suitable for X-ray diffraction were obtained by cooling their hexane solutions at ca. −17 °C. Yield: 0.836 g (0.76 mmol, 52.0%); mp 273−276 °C; ^{1}H NMR (599.7 MHz, C_6D_6, 295 K): δ = 1.12 (d, 24H, *o*-CH(C*H*$_3$)$_2$, $^3J_{H,H}$ = 7.04 Hz), 1.27 (d, 24H, *o*-CH(C*H*$_3$)$_2$, $^3J_{H,H}$ = 7.04 Hz), 1.32 (d, 24H, *p*-CH(C*H*$_3$)$_2$, $^3J_{H,H}$ = 7.04 Hz), 2.78 (m, 8H, *o*-C*H*(CH$_3$)$_2$, $^3J_{H,H}$ = 6.75 Hz), 2.90 (m, 4H, *p*-C*H*(CH$_3$)$_2$, $^3J_{H,H}$ = 7.04 Hz), 6.91 (t, 2H, *p*-C_6H_3, $^3J_{H,H}$ = 7.49 Hz), 7.04 (d, 4H, *m*-C_6H_3, $^3J_{H,H}$ = 7.63 Hz), 7.12 (s, 8H, *m*-$C_6H_2Pr^i_3$); ^{13}C{^{1}H} NMR (C_6D_6, 150.8 MHz, 295 K): δ = 23.69 (*o*-CH(*C*H$_3$)$_2$), 24.47 (*o*-CH(*C*H$_3$)$_2$), 25.50 (*o*-CH(*C*H$_3$)$_2$), 31.23 (*p*-CH(*C*H$_3$)$_2$), 34.75 (*p*-C*H*(CH$_3$)$_2$), 121.59 (*p*-C_6H_3), 124.64 (*m*-$C_6H_2Pr^i_3$), 129.90 (*m*-C_6H_3), 137.25 (*o*-C_6H_3), 138.82 (*o*-$C_6H_2Pr^i_3$), 141.19 (*p*-$C_6H_2Pr^i_3$), 146.99 (*i*-$C_6H_2Pr^i_3$), 148.91 (*i*-C_6H_3); UV−vis: [λ, nm (ε, M^{-1}cm^{-1})] 414 (3600), 338 (3700), 286 (4100); IR (cm^{-1}): The Ge−S stretching band was tentatively assigned to an absorption at 438 cm^{-1}.

The germylenes Ge(SAr^{Me_6})$_2$ (**4**) and Ge(SAr$^{Pr^i_8}$)$_2$ (**7**) were prepared by a similar method to that used for **5**. See Supporting Information for details.

*Sn(SAr^{Me_6})$_2$ (**8**).* LiSAr^{Me_6} (1.120 g, 3.18 mmol) was dissolved in ca. 60 mL of diethyl ether and added dropwise over 30 min to a diethyl ether (5 mL) slurry of $SnCl_2$ (0.301 g, 1.59 mmol) cooled to ca. −78 °C. The solution immediately became yellow and was stirred at ca. −78 °C for a further 30 min and then allowed to warm slowly to a room temperature. The solution was stirred for 24 h to give a yellow solution and a white precipitate. All the volatile components were removed under reduced pressure. Toluene (50 mL) was added and filtration afforded a clear, yellow solution. The filtrate was concentrated under reduced pressure to a ca. 12 mL and placed in a ca. −17 °C freezer to afford X-ray quality crystals of **8** as pale-yellow blocks after 3 days. Yield: 0.404 g (0.50 mmol, 31.4%); mp 194−196 °C. Calcd for $C_{48}H_{50}S_2Sn$: C, 71.20; H, 8.74. Found: C, 70.93; H, 8.49. ^{1}H NMR (300.1 MHz, C_6D_6, 298 K): δ = 2.06 (s, 24H, *o*-CH$_3$), 2.17 (s, 12H, *p*-CH$_3$), 6.78 (s, 8H, $C_6H_2Me_3$), 6.85 (d, 4H, *m*-C_6H_3, $^3J_{H,H}$ = 7.50 Hz), 7.00 (t, 2H, *p*-C_6H_3, $^3J_{H,H}$ = 7.50 Hz); ^{13}C{^{1}H} NMR (C_6D_6, 75.45 MHz, 298 K): δ = 20.27 (*p*-CH$_3$), 21.23 (*o*-CH$_3$) 124.78 (*p*-C_6H_3), 125.46 (*m*-$C_6H_2Me_3$), 129.35(*m*-C_6H_3), 136.31 (*o*-C_6H_3), 137.11 (*o*-$C_6H_2Me_3$), 137.47 (*p*-$C_6H_2Me_3$), 140.03 (*i*- $C_6H_2Me_3$), 142.58 (*i*-C_6H_3); ^{119}Sn NMR (223.6 MHz, C_6D_6, 295 K): δ = 763.8; UV−vis: [λ, nm (ε, M^{-1}cm^{-1})] 400 (1100), 298 (5300), 292 (5300); IR (cm^{-1}): Sn−S stretching band tentatively assigned to an absorption at 393 cm^{-1}.

The stannylenes, Sn(SAr$^{Pr^i_4}$)$_2$ (**9**), Sn(SAr$^{Pr^i_6}$)$_2$ (**10**), and Sn(SAr$^{Pr^i_8}$)$_2$ (**11**) were prepared by a similar method to that used for **8**, see Supporting Information for details.

*Pb(SAr$^{Pr^i_8}$)$_2$ (**14**).* LiSAr$^{Pr^i_8}$ (0.952 g, 1.56 mmol; see compound **33**, SI) and $PbBr_2$ (0.289 g, 0.79 mmol) were placed in a flask, and diethyl ether (60 mL) cooled to ca. −78 °C was added. The resulting solution was stirred at ca. −78 °C for 2 h and warmed to ca. 25 °C. It was stirred for a further 24 h to give an orange-red solution and a white precipitate. All of the volatile components were removed under reduced pressure. The product was extracted with pentane (100 mL) and filtered. The filtrate was concentrated under reduced pressure to a ca. 20 mL and placed in a ca. −17 °C freezer, which afforded a small quantity of X-ray quality crystals of the disulfide, (SAr$^{Pr^i_8}$)$_2$ as yellow rods after 3 days. The supernatant liquid was decanted and further concentrated to 8 mL and placed in a ca. −17 °C freezer for 2 weeks to afford X-ray quality crystals of **14** as orange rods. Yield: 0.450 g (0.321 mmol 40.8%); mp 246−249 °C; ^{1}H NMR (599.7 MHz, C_6D_6, 295 K): δ = 1.14 (d, 24H, *o*-CH(C*H*$_3$)$_2$, $^3J_{H,H}$ = 6.63 Hz), 1.25 (d, 24H, *m*-CH(C*H*$_3$)$_2$, $^3J_{H,H}$ = 6.96 Hz), 1.34 (d, 24H, *p*-CH(C*H*$_3$)$_2$, $^3J_{H,H}$ = 6.97 Hz), 1.41 (d, 24H, *o*-CH(C*H*$_3$)$_2$, $^3J_{H,H}$ = 6.63 Hz), 2.60 (m, 8H, *o*-CH(C*H*$_3$)$_2$, $^3J_{H,H}$ = 6.64 Hz), 2.88 (m, 8H, *p*-CH(C*H*$_3$)$_2$, $^3J_{H,H}$ = 6.97 Hz), 2.90 (m, 8H, *o*-CH(C*H*$_3$)$_2$, $^3J_{H,H}$ = 6.63 Hz), 7.18 (s, 2H, *p*-C_6H_3), 7.24 (s, 8H, *m*-C_6H_3,); ^{13}C{^{1}H} NMR (C_6D_6, 150.8 MHz, 295 K): δ = 24.29 (CH(*C*H$_3$)$_2$), 24.42 (CH(*C*H$_3$)$_2$), 24.83 (CH(*C*H$_3$)$_2$), 25.07 (CH-(*C*H$_3$)$_2$), 26.43 (CH(*C*H$_3$)$_2$), 26.55 (CH(*C*H$_3$)$_2$), 31.21 (*C*H(CH$_3$)$_2$), 121.89 (*p*-$C_6HPr^i_2$), 122.12 (*m*-$C_6H_2Pr^i_3$), 136.94 (*m*-$C_6HPr^i_2$), 140.29 (*o*-$C_6HPr^i_2$), 141.30 (*p*-$C_6H_2Pr^i_3$), 146.69 (*o*-$C_6H_2Pr^i_3$), 147.73 (*i*-$C_6H_2Pr^i_3$), 149.13 (*i*-$C_6HPr^i_2$); ^{207}Pb{^{1}H} NMR (125.53 MHz, C_6D_6, 295 K): δ = 4335; UV−vis: [λ, nm (ε, M^{-1}cm^{-1})] 446 (4200), 372 (2500), 292 (6600); IR (cm^{-1}): The Pb−S stretching band was tentatively assigned to an absorption at 302 cm^{-1}.

Pb(SAr$^{Pr^i_6}$)$_2$ (**13**) was prepared by a similar method to **14**, see SI for details.

*Ge(SeAr$^{Pr^i_4}$)$_2$ (**15**).* LiSeAr$^{Pr^i_4}$ (1.21 g, 2.50 mmol) in diethyl ether (40 mL) was added dropwise over 15 min to a diethyl ether slurry (5 mL) of $GeCl_2$(1,4-dioxane) (0.290 g, 1.25 mmol) cooled to −72 °C. The solution became a bright-orange color immediately, and after 1 h, it was allowed to warm to ambient temperature and was stirred overnight. All the volatile components were removed under reduced pressure, and the residue was extracted with *n*-pentane (50 mL) and filtered. The solution was concentrated to ca. 3 mL, warmed gently, and allowed to sit at ambient temperature overnight to produce X-ray quality amber crystals of **15**. Calcd for $C_{60}H_{74}GeSe_2$: C, 70.26; H, 7.27. Found: C, 70.7; H, 7.27. Yield: 0.710 g (0.690 mmol, 53.7%); mp 205−207 °C; ^{1}H NMR (599.7 MHz, C_6D_6, 295 K): δ = 1.05 (d, 24H, *o*-CH(C*H*$_3$)$_2$, $^3J_{H,H}$ = 6.75 Hz), 1.22 (d, 24H, *o*-CH(C*H*$_3$)$_2$, $^3J_{H,H}$ = 6.75 Hz), 2.77 (m, 8H, *o*-C*H*(CH$_3$)$_2$, $^3J_{H,H}$ = 7.04 Hz), 6.99 (t, 2H, *p*-C_6H_3, $^3J_{H,H}$ = 8.22 Hz), 7.02 (d, 4H, *m*-C_6H_3, $^3J_{H,H}$ = 7.92 Hz), 7.09 (d, 8H, *m*-$C_6H_2Pr^i_2$, $^3J_{H,H}$ = 7.63 Hz), 7.19 (t, 4H, *p*-$C_6H_2Pr^i_2$, $^3J_{H,H}$ = 7.63 Hz); ^{13}C{^{1}H} NMR (C_6D_6, 150.8 MHz, 295 K): δ = 23.73 (*o*-CH(*C*H$_3$)$_2$), 25.16 (*o*-CH(*C*H$_3$)$_2$), 31.15 (*o*-C*H*(CH$_3$)$_2$), 123.92, (*m*-$C_6H_2Pr^i_3$), 125.36 (*p*-C_6H_3), 129.02 (*m*-C_6H_3), 129.47 (*o*-C_6H_3), 138.38 (*p*-$C_6H_2Pr^i_2$), 140.43 (*o*-$C_6H_2Pr^i_2$), 142.77 (*i*-$C_6H_2Pr^i_2$), 146.74 (*i*-C_6H_3); ^{77}Se NMR (114.4 MHz, C_6D_6, 295 K): δ = 657.5; UV−vis: [λ, nm (ε, M^{-1}cm^{-1})] 435 (7700), 358 (9000), 303 (8900).

*Sn(SeAr$^{Pr^i_4}$)$_2$ (**16**).* Stannylene **16** was prepared by a similar method to that of **15**, except that potassium selenolate was used instead of the lithium selenolate, see SI for details.

X-ray Crystallography. Crystals of **2**, **7**−**11**, **13**−**16**, **27**, **28**, and **30**−**35** were removed from a Schlenk tube under N_2 and covered with a layer of hydrocarbon oil. A suitable crystal was selected, attached to a glass fiber, and quickly placed in low temperature N_2 stream. The data for **2**−**11**, **13**−**16**, **27**, **28**, and **30**−**35** were collected at ca. 90 K on a Bruker APEX II CCD or Bruker DUO APEX II CCD diffractometers with Mo Kα (λ = 0.71073 Å) radiation or Cu Kα (λ = 1.5418 Å). The crystal structures were solved by direct methods using SHELX version 6.1 program package.[20,21] All nonhydrogen atoms were refined anisotropically. Absorption corrections were applied using SADABS

dx.doi.org/10.1021/ja403802a | J. Am. Chem. Soc. XXXX, XXX, XXX−XXX

program (SADABS, an empirical absorption correction programs, part of the SAINTPlus NT version 5.0 package; Bruker AXS: Madison, WI, 1998). All crystallographic calculations were performed on an iMac with 2.80 GHz i7 quad core processor and 8GB of memory. Data collected were corrected for Lorentz and polarization effects and absorption using Blessing's method and merged as incorporated into the program Twinabs. Structures were drawn using the program OLEX2.[22a] Details of the data collections and refinements are given in the SI (Tables S3-S6). For **2**, the potassium thiolate salt $(KSAr^{Pr^i_4})_2$ (**31**; see SI) was used in a cocrystallization with the silicon dithiolate $Si(SAr^{Pr^i_4})_2$ (**2**) to facilitate the structural determination of **2**, although we later found that crystals of **2** suitable for X-ray crystallography could also be obtained from toluene solvent. The structure of the potassium salt (**31**) was also determined from an independently synthesized sample, as was the structure of the $Si(Br)_2(SAr^{Pr^i_4})_2$ (**27**), which was a 5% contaminant. X-ray data for the $Ar^{Pr^i_6}$ substituted thiolate derivatives **3** and **6** were also obtained. The data refinement for these two structures could not be performed to low residual values, although the key structural parameters for the core atoms could be obtained without difficulty. It is noteworthy that the $Ar^{Pr^i_6}$ terphenyl substituent has also been associated with difficulties in the refinement of X-ray data for other systems.[22b] Some key structural data for the core atoms in these structures are given in Table 2, where it can be seen that their structural parameters conform to the pattern established by the structures of the other compounds in the series.

Mössbauer Spectroscopy. Experimental samples were shipped in sealed ampules, transferred (ca. 45 s) to O-ring-sealed sample holders in an inert atmosphere glovebox, and quenched to liquid nitrogen temperature prior to mounting in the precooled cryostat. They were examined in transmission geometry using a 10 mCi $CaSnO_3$ source at room temperature as previously described, as was the spectrometer calibration.[23] The Mössbauer effect (ME) data were collected over the temperature range $\sim 90 < T < 220$ K. Sample temperature was monitored using the Daswin program,[23b] and the transmission data were monitored (to ensure no sample loss) before and after each temperature data point acquisition.

Computational Details. All calculations were performed with the Turbomole 6.3 program package[24a] and the results were visualized with gOpenMol.[24b,c] The geometries of R−Ch−M−Ch−R, where M = Si, Ge, Sn, Pb; Ch = O, S, Se; and R = H, Ph, C_6H_3-2,6-Ph_2, $Ar^{Pr^i_8}$ were optimized with the hybrid PBE1PBE density functional[25] in combination with the TZVP basis sets.[26] Due to the size of the systems in question, frequency calculations were performed only for R = H, Ph derivatives to assess the nature of stationary points found. The structures with R = $Ar^{Pr^i_8}$ substituents were also optimized using Grimme's empirical dispersion correction scheme (DFT-D3).[27]

RESULTS AND DISCUSSION

Synthesis. As recently shown, the silylene, $Si(SAr^{Me_6})_2$ (**1**) was synthesized by reduction of $Br_2Si(SAr^{Me_6})_2$ with $(IMesMg)_2$ (IMes = $[(2,4,6\text{-trimethylphenyl})NC(CH_3)]_2CH$).[12] However, attempts to extend this method to the more sterically crowded silylenes $Si(SAr^{Pr^i_4})_2$ (**2**) and $Si(SAr^{Pr^i_6})_2$ (**3**) were unsuccessful. This is likely due to the increased steric hindrance of the bulkier terphenyl ligands. Instead, the dibromo-bisthiolato Si(IV) precursors, $Br_2Si(SAr^{Pr^i_4})_2$ and $Br_2Si(SAr^{Pr^i_6})_2$, were reduced using magnesium (as prepared by Rieke)[15] with a catalytic amount of anthracene to yield the new acyclic silylenes, $Si(SAr^{Pr^i_4})_2$ (**2**) and $Si(SAr^{Pr^i_6})_2$ (**3**). Attempts to synthesize $Si(SAr^{Me_6})_2$, by reduction using only Rieke's magnesium, were unsuccessful. Based on ^{29}Si NMR evidence (signal at $\delta = 50.5$), we believe that a magnesium bromide-bisthiolato-bromosilylenoid, $SiBr(MgBr)(SAr^{Me_6})_2$, was formed instead.[12,28,29] A previously reported magnesium silylenoid, SiBr(Mes)(Tsi)(MgBr) (Mes = 2,4,6-C_6H_2-Me_3, Tsi = $C(SiMe_3)_3$) was assigned a shift of $\delta = 140.5$ in the ^{29}Si NMR spectrum.[30] The upfield shift of $SiBr(MgBr)(SAr^{Me_6})_2$ is probably due to the more electronegative thiolate substituents. The silylenoid is likely an intermediate in the synthesis of silylenes **2** and **3**; however, in those systems, the $MgBr_2$ is apparently eliminated, possibly due to increased steric crowding of the bulkier ligands (SI).

The syntheses of most of the Ge−Pb aryloxo and arylthiolato complexes were carried out primarily by a salt metathesis of the lithium or potassium chalcogenolates with the corresponding metal dihalide. An exchange reaction using $Sn\{N(SiMe_3)_2\}_2$ with 2 equiv of the corresponding thiol was also used as an alternative synthetic route to $Sn(SAr^{Pr^i_8})_2$. Previous work by Clyburne to determine the structure of the complex $Ge(OAr^{Me_6})_2$ proved unsuccessful due to poor crystallinity, although a structure of $Sn(OAr^{Me_6})_2$ was obtained.[31] An overview of the synthesis of **2**−**20** is given in Scheme 1.

During the synthesis of $M(SAr^{Pr^i_8})_2$ or $M(SeAr^{Pr^i_4})_2$, (M = Sn, Pb) small amounts of the disulfide $(Ar^{Pr^i_8}S)_2$ and diselenide $(Ar^{Pr^i_4}Se)_2$ were observed as coproducts. Furthermore, solutions of $Sn(SAr^{Pr^i_8})_2$ deposit tin metal and the disulfide $(SAr^{Pr^i_8})_2$ upon standing at ca. 25 °C over a period of several months. This is similar to reports of other group 14 dithiolate oligomers that have been shown to decompose over time, although those resulted in the formation of the metal sulfide and diaryl sulfide.[32] The decomposition pathways may differ because of the greater steric hindrance associated with the terphenyl ligands.

Structures. *Dithiolates.* The most numerous of the divalent species discussed in this paper are the dithiolato derivatives of Si, Ge, Sn and Pb, **1**−**14**, and their structures are described first. Important structural data for **1**−**14** are given in Table 1 which also includes data for the stannylene, $Sn(SMes^*)_2$, (Mes* = C_6H_2-2,4,6-Bu^t_3, **26**) for comparison.[9] The most notable feature of the structures is that with the exception of $Si(SAr^{Me_6})_2$, (S−Si−S = 90.52(2)°),[12] they all possess S−M−S bond angles below 90°. Furthermore, and in contrast to the usual expectation,[6,33] as the bulk of the aryl substituents increases in the silicon, germanium, and tin dithiolates, the S−M−S bond angle decreases. In contrast, the S−Pb−S angles change little when the size of the substituents is varied. The data in Table 1 also show that, as the crowding of the terphenyl ligand increases, as in $SAr^{Me_6} < SAr^{Pr^i_4} < SAr^{Pr^i_6} < SAr^{Pr^i_8}$, the angle (M−S−C−C) between the plane of the central aryl ring of the terphenyl ligand and the M−S−$C_{(ipso)}$ plane decreases. (this is accompanied by decreased interligand distances between the Pr^i substituents; Table 33, SI). This is also contrary to steric expectations. However, the torsion angle between the S−$C_{(ipso)}$ bond and the S−M−S plane (C−S−M−S) does not display a correlation with the size of the terphenyl ligand, with the majority of the angles having values between 20° and 30°. The structures of the compounds of the thiolate series are illustrated by the tin derivatives shown in Figure 2 as well as the silylenes $Si(SAr^{Me_6})_2$ and $Si(SAr^{Pr^i_4})_2$ in Figure 3.

The average Si−S distance in silylenes **2** (2.137(1) Å) and **3** (2.089(9) Å) is slightly shorter than that in **1** (2.158(3) Å) and is comparable to those found in Tilley's bisthiolatosilylene platinum complex, *trans*-$(Cy_3P)_2Pt(H)Si(SEt)_2OTf$ (2.092(4) and 2.074(4) Å),[34a] whereas the S−Si−S angles in **1**−**3** are all significantly narrower by more than 17°. Likewise, the Ge−S distances and S−Ge−S angles in germylenes **4**−**7** are both longer

dx.doi.org/10.1021/ja403802a | J. Am. Chem. Soc. XXXX, XXX, XXX−XXX

Scheme 1. Overview of the Synthesis of 2−20[a]

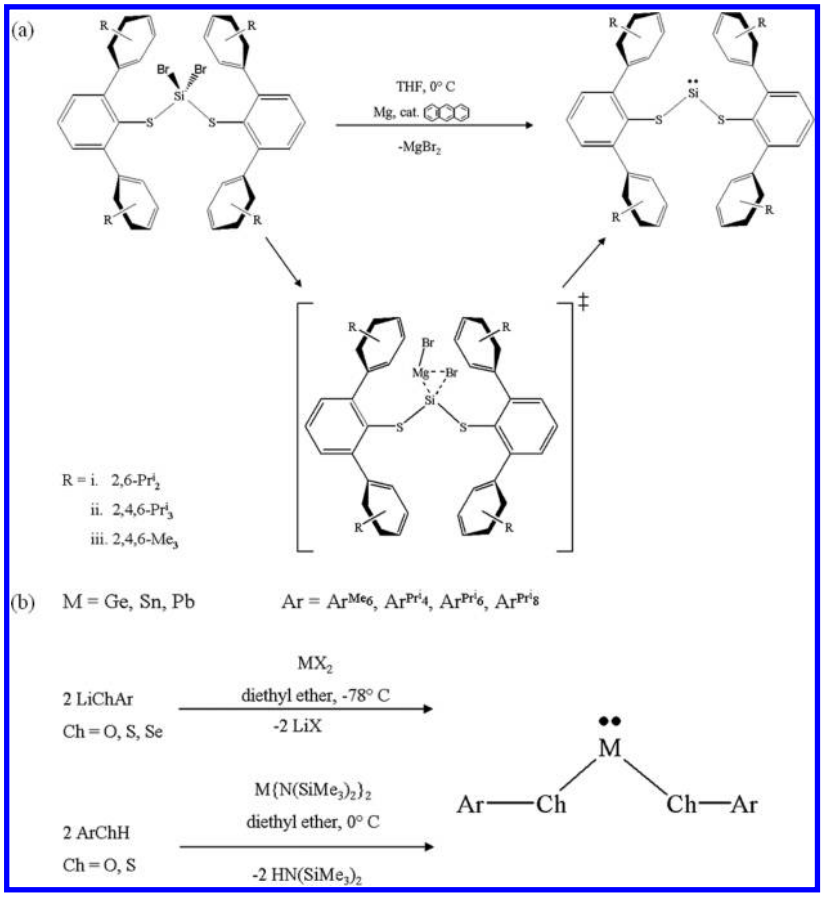

[a](a) Reduction of dibromo-bisthiolato-silanes with magnesium anthracenide gives the silylene analogues (i, ii). Reduction by Rieke's magnesium is believed to proceed through a magnesium silylenoid intermediate (iii). (b) A general overview of the synthetic routes for the synthesis of very bulky germylene, stannylene, and plumbylene dichalcogenolates.

Table 1. Selected Distances (Å) and Angles (°) for $M(SAr)_2$ (M = Si, Ge, Sn, Pb) Dithiolato Compounds

compound	S−M	S−M−S	M−C−S	M−S−C−C	C−S−M−S	C−S	M-centroid	S···S	ref
(**1**) $Si(SAr^{Me_6})_2$	2.158(3)[a]	90.52(2)	102.93(6)[a]	44.9(1)[a]	15.5/11.3	1.791(2)[a]	3.431[a]	3.0666(4)	12
(**2**) $Si(SAr^{Pr^i_4})_2$	2.137(1)	85.08(5)	113.80(9)	38.2(2)	26.6	1.775(2)	3.249	2.8903(9)	this work
(**3**) $Si(SAr^{Pr^i_6})_2$[b]	2.089(9)[a]	84.8(1)[a]	118.(1)[a]	29(7)[a]	29.9/30.0	1.77(1)	3.31(6)[a]	2.817(3)[a]	this work
(**4**) $Ge(SAr^{Me_6})_2$	2.265(1)[a]	88.68(2)	103(3)[a]	40(6)[a]	23.0	1.785(1)[a]	3.28(5)[a]	3.1656(6)	this work
(**5**) $Ge(SAr^{Pr^i_4})_2$	2.284(4)	81.26(2)	113.58(5)	32.3(1)	28.0	1.778(1)	3.094	2.9749(6)	this work
(**6**) $Ge(SAr^{Pr^i_6})_2$[b]	2.24(4)[a]	79.6(2)	114(1)[a]	27(7)[a]	25.5/26.1	1.79(3)[a]	3.3(1)[a]	2.867(7)	this work
(**7**) $Ge(SAr^{Pr^i_8})_2$	2.2940(6)	77.01(2)	119.42(6)	3.6(2)	27.3	1.782(2)[a]	3.302	2.8566(6)	this work
(**26**) $Sn(SMes^*)_2$	2.4356(3)	85.4(1)	101.64	86.34	9.6	1.8087(2)	4.383	3.3034(5)	9
(**8**) $Sn(SAr^{Me_6})_2$	2.479(5)[a]	85.555(3)	104(5)[a]	38(10)[a]	19.6/20/7	1.7815(9)[a]	3.22(9)	3.3677(4)	this work
(**9**) $Sn(SAr^{Pr^i_4})_2$	2.470(1)	78.63(3)	113.8(1)[a]	31.2(3)[a]	29.3	1.778(4)[a]	3.082[a]	3.130(1)	this work
(**10**) $Sn(SAr^{Pr^i_6})_2$	2.46(6)[a]	78.2(2)[a]	113(1)[a]	34(6)[a]	23.4−31.1	1.774(2)[a]	3.3(2)[a]	3.10(2)[a]	this work
(**11**) $Sn(SAr^{Pr^i_8})_2$	2.5009(6)	73.09(2)	119.15(8)	3.8(2)	27.5	1.776(2)	3.220	2.9783(8)	this work
(**12**) $Pb(SAr^{Pr^i_4})_2$	2.5656(9)	77.21(4)	113.42(11)	31.0(1)	29.8	1.771(3)	3.046	3.202(1)	11
(**13**) $Pb(SAr^{Pr^i_6})_2$	2.579(5)[a]	77.27(2)	114.9(7)[a]	28(8)[a]	27.1/33.8	1.772(2)[a]	3.12(5)[a]	3.2207(7)	this work
(**14**) $Pb(SAr^{Pr^i_8})_2$	2.587(7)[a]	80.07(2)	117.4(9)[a]	29(4)[a]	30.2/34.7	1.782(1)[a]	3.08(2)[a]	3.3281(7)	this work

[a]Averaged values. [b]Data for these two structures could not be refined to a low residual value.

(ca. 2.24- 2.29 Å) and narrower (ca. 89−77°) than those of Jutzi's bisthiolatogermylene chromium complex, $Cr(CO)_5Ge(SC_6H_2$-2,4,6-$Me_3)_2$, that has Ge−S distances of 2.181(4) and 2.192(6) Å and a S−Ge−S angle of 102.4(2)°.[34b] The S−Sn−S angle in $Sn(SAr^{Me_6})_2$ (**8**, 85.553(3)°) is similar to the 85.4(1)° in Lappert's $Sn(SMes^*)_2$ (**26**) (where the sub-90° angle was deemed not to be due to steric effects),[9] but the interligand angles become narrower in the bulkier stannylenes **9** (78.63(3)°), **10** (78.2(2)°), and **11** (73.09(2)°). The Ge−S distances in **4**−**7** (range: 2.265(1)−2.2940(6) Å) are ca. 0.05−0.07 Å longer than the ca. 2.22 Å typically observed in Ge(IV) thiolates.[35a] The Sn−S bond lengths in **8**−**11** (2.46(6)−2.5009(6) Å) are longer than those in Sn(IV) thiolates (e.g., 2.382(1) Å in $Sn(SC_6H_{11})_4$ and 2.397(1) Å in $Sn(SBu^t)_4$.[35b]

dx.doi.org/10.1021/ja403802a | J. Am. Chem. Soc. XXXX, XXX, XXX−XXX

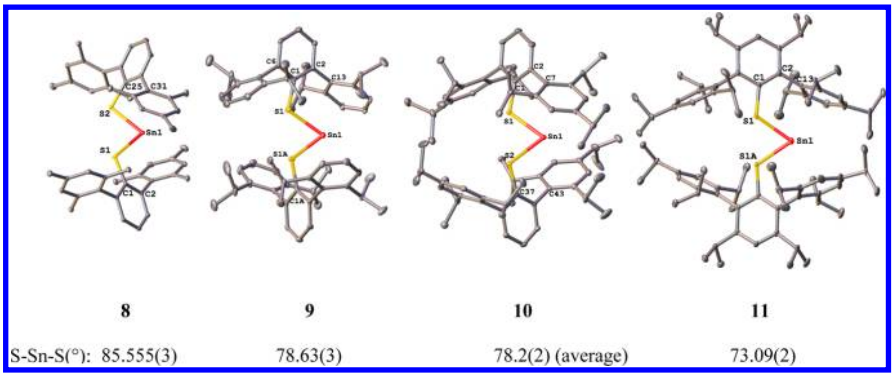

Figure 2. Thermal ellipsoid drawings (30% probability ellipsoids without hydrogen atoms) of the Sn(II) derivatives of the SAr^{Me_6} (**8**), $SAr^{Pr^i_4}$ (**9**), $SAr^{Pr^i_6}$ (**10**), and $SAr^{Pr^i_8}$ (**11**) thiolato ligands, showing that the bulkiest ligand, $SAr^{Pr^i_8}$, yields a narrower (73.09(2)°) S−Sn−S bond angle in comparison to the 85.553(3)° observed for the smallest SAr^{Me_6} ligand. The essential coplanarity of the central aryl ring of the terphenyl substituents within the SnS_2 core structure is apparent in the structure of **11**.

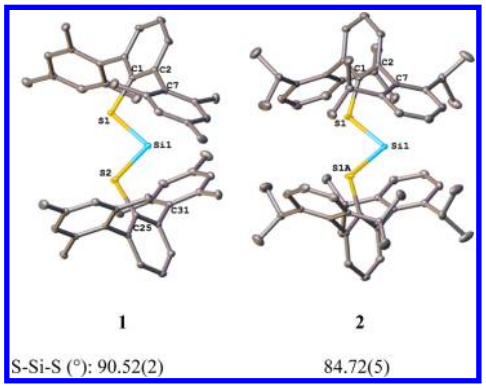

Figure 3. Thermal ellipsoid (30%) drawings of the structures of **1** and **2**; hydrogens are not shown for clarity. The structure of **2** features the narrowest R−Si−R angle (84.72(5)°) for a two-coordinate silylene (cyclic or acyclic).

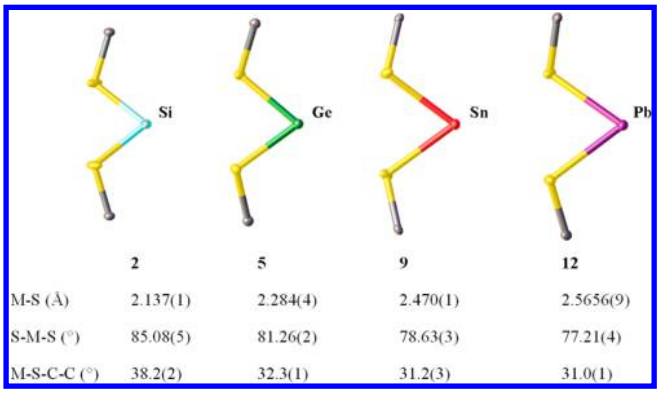

Figure 4. Drawings of the core atoms in the bisthiolato tetrylenes $M(SAr^{Pr^i_4})_2$ (M = Si, **2**; Ge, **5**; Sn, **9**; Pb, **12**) (30% probability ellipsoids) which feature identical $SAr^{Pr^i_4}$ ligands and show that the S−M−S angle becomes narrower with increasing atomic number.

Presumably the longer distances in **4**−**11** are mainly due to the larger sizes of the Ge^{2+} and Sn^{2+} ions and the changed polar character of the bonds.

In contrast to the silylene, germylene, and stannylene derivatives, the plumbylene dithiolates displayed only minor variation (ca. 2.9°) in their S−M−S angles with the different terphenyl substituent sizes. The M−S−C−C torsion angles, of the lead thiolates, also remain relatively constant at ca. 29°. We attribute the lower angular/substituent dependence to the larger size of lead in comparison to the lighter elements. In the lead derivatives, the Pb−S bonds lengthen slightly with increasing substituent size and in all cases,[11] the Pb−S distances in plumbylenes **12**−**14** are longer than the Pb−S distance found in Tokitoh's monothiolato plumbylene, Pb(Tbt)(STbt), (Tbt = C_6H_2-2,4,6-$(CH(SiMe_3)_2)_3$) (2.498(10) Å).[36] The C−S bond lengths are very similar to those seen in the lighter analogues with an almost negligible average decrease of about 0.01 Å upon descending the group.[37]

Although not all of the structures of the compounds of the thiolate series are currently known, the structural data clearly display patterns that can be summarized as follows:

(1) The S−M−S interligand angles for M = Si, Ge and Sn derivatives decrease as the bulk of the terphenyl substituents increases.
(2) The S−M−S interligand angles decrease in the order M = Si > Ge > Sn > Pb (Figure 4).
(3) The M−S−$C_{(ipso)}$ bending angles of the thiolate ligands increase as the size of the terphenyl substituents increases for all compounds including those of lead.
(4) The M−S−C−C torsion angles decrease with increasing size of the terphenyl substituents except in the lead derivatives where it changes little. This results in the opposition of flanking ring isopropyl substituents from the two terphenyl substituents across the axis of the molecule, contrary to steric expectations.
(5) The M−S bond lengths for each element display only minor variation with terphenyl substituent size.
(6) The $C_{(ipso)}$−S bond lengths vary little throughout the series.

The most striking features of the structural data are the decreasing interligand Ch−M−Ch and M−Ch−C−C angles as the terphenyl substituent size increases for the Si, Ge, and Sn derivatives. These trends are counterintuitive from the point of view of purely steric considerations. Clearly, other factors influence the structures, and these will be discussed below.

Aryloxo and Selenolato Derivatives. Selected structural data for aryloxo and selenolato derivatives are given in Tables 2 and 3. The tetrylenes, $Ge(SeAr^{Pr^i_4})_2$ (**15**, Figure 5) and $Sn(SeAr^{Pr^i_4})_2$ (**16**), are the first structurally characterized two-coordinate Ge(II) and Sn(II) selenolates and rare examples of two-coordinate metallylenes stabilized by ligands bonded through fourth row elements.[6,38]

dx.doi.org/10.1021/ja403802a | J. Am. Chem. Soc. XXXX, XXX, XXX−XXX

Table 2. Selected Distances (Å) and Angles (°) for $M(OAr)_2$ (M = Ge, Sn, Pb) Compounds

compound[b]	O−M	O−M−O	C−O−M	M−O−C−C	C−O	M-centroid	O···O	ref
(**17**) $Ge(OAr^{Pr^i_4})_2$	1.8271(16)[a]	92.54(6)	128.03(13)[a]	36.9(4)[a]	1.378(3)[a]	3.377[a]	2.640(2)	40
(**18**) $Sn(OAr^{Me_6})_2$	2.041(3)[a]	87.32(11)	126.7(3)[a]	30.0[a]	1.343(6)[a]	2.961[a]	2.818(5)	31
(**19**) $Sn(OAr^{Pr^i_4})_2$	2.0472(17)[a]	92.18(6)	129.25(15)[a]	30.6[a]	1.360(3)[a]	3.163[a]	3.13	40
(**20**) $Pb(OAr^{Pr^i_4})_2$	2.216(8)[a]	99(1)[a]	127(2)[a]	26(5)	1.354(2)[a]	2.95(3)[a]	3.38(3)[a]	11
(**21**) $Ge(OAr^*Me)_2$	1.807(9)[a]	92.0(4)	124.7(7)[a]		1.44(2)[a]			8a
(**22**) $Sn(OAr^*Me)_2$	2.009(5)[a]	88.8(2)	125.2(5)[a]		1.371(7)[a]			8a
(**23**) $Pb(OAr^*Me)_2$	2.14(2)[a]	86.2(4)	124(2)[a]		1.36(1)[a]			8b
(**24**) $Ge\{OC_6H_3\text{-}2,6\text{-}Ph_2\}_2$	1.820(3)[a]	92.10(5)	117.2(2)					8c
(**25**) $Ge\{OC_6H\text{-}2,3,5,6\text{-}Ph_4\}_2$	1.820(1)	91.09(7)	124.1(1)					8c

[a]Average value. [b]$Ar^*Me = C_6H_2Bu^t_2$-2,6-Me-4.

Table 3. Selected Distances (Å) and Angles (°) for Compounds $M(SeAr)_2$, M = Ge, Sn

compound	Se−M	Se−M−Se	C−Se−M	M−Se−C−C	C−Se	M-centroid	Se···Se	ref
(**15**) $Ge(SeAr^{Pr^i_4})_2$	2.396(5)[a]	84.715(1)	108.8(5)[a]	36(1)[a]	1.939(4)[a]	3.17(3)[a]	3.2301(6)	this work
(**16**) $Sn(SeAr^{Pr^i_4})_2$	2.594(3)[a]	78.60(3)	112.1(3)[a]	26(7)[a]	1.935(9)[a]	3.17(7)[a]	3.286(1)	this work

[a]Average value.

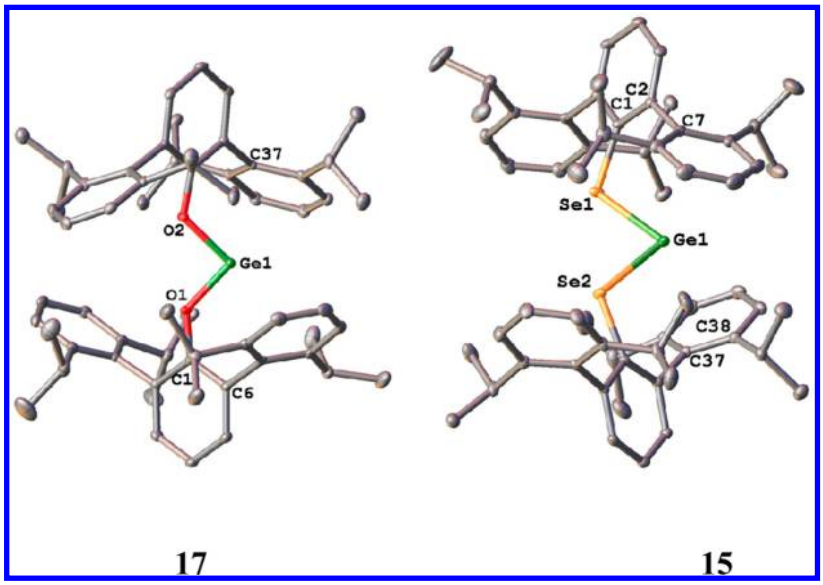

Figure 5. X-ray structures of the bisphenoxo and bisselenolato germylenes **17** and **15** (30% probability ellipsoids) without hydrogen atoms. The Ch−Ge−Ch angles are: O1−Ge1−O2 = 92.54(6)°; Se1−Ge1−Se2 = 84.75(1)°. Other structural data are given in Table 4.

The structural data for the selenolates are necessarily limited because of their lower stability in comparison to the aryloxides or thiolates which is presumably a result of the decreased M−Se bond strengths.[39a] The compounds, $Ge(SeAr^{Pr^i_4})_2$ and $Sn(SeAr^{Pr^i_4})_2$, have group 14 element−selenium bonds that are 0.11 and 0.12 Å longer than their thiolate counterparts. The increase corresponds roughly to the 0.13 Å difference in the single bond covalent radii of S and Se.[37] The Se−Ge−Se angle in $Ge(SeAr^{Pr^i_4})_2$ is about 3.5° wider than the S−Ge−S angle in $Ge(SAr^{Pr^i_4})_2$, and the Ge−Se−C angle is about 4.8° narrower. In the tin complexes, $Sn(SAr^{Pr^i_4})_2$ and $Sn(SeAr^{Pr^i_4})_2$, the Ch−Sn−Ch and Sn−C−Ch angles are very similar (78.63(3) and 31.2(3) for $SAr^{Pr^i_4}$ vs 78.60(3) and 26(7)°). As in the Ge(II) thiolates discussed above, the Ge−Se bond length in **15** is longer than those seen in the Ge(IV) selenolates (e.g., $Ge(SeMes)_4$, 2.37(1) Å).[8c,39b]

In Table 2, it can be seen that the aryloxo derivatives are characterized by O−M−O angles (cf. **17** in Figure 5) that are significantly wider than the corresponding S−M−S and Se−M−Se angles.[8,31,40]

Table 4 gives structural details of all the available divalent, group 14 element aryloxo, thiolate and selenolato metallylenes that carry the common terphenyl substituent ($Ar^{Pr^i_4}$). A similar range of structural data is not currently available for the other terphenyl substituents. The Ch−M−Ch angles for the terphenyloxo complexes are wider than those of the thiolato and selenolato derivatives by ca. 11.3° for germanium, ca. 1.77−13.55° for tin, and ca. 22° for lead complexes. The deviation of the Ch−M−Ch angle from 90° is largest for S and Se derivatives. The more electronegative aryloxide derivatives feature the widest interligand angles that are seemingly in contradiction of Bent's rule.[7]

The structure of $Sn(SAr^{Pr^i_6})_2$ (**10**) is worthy of further comment: it contains two molecules in the asymmetric unit possessing similar S−Sn−S angles of 78.27(1)° and 78.1(2)° and Sn−S−C-C torsion angles of 30(2)° and 36(7)°, respectively, but one of the molecules

dx.doi.org/10.1021/ja403802a | J. Am. Chem. Soc. XXXX, XXX, XXX−XXX

Table 4. Selected Distances (Å) and Angles (°) for $ChAr^{Pr^i_4}$ Substituted Derivatives, M = Ge, Sn, Pb

		$OAr^{Pr^i_4}$	$SAr^{Pr^i_4}$	$SeAr^{Pr^i_4}$
Ge	Ge−Ch	(**17**) 1.827(16)	(**5**) 2.284(4)	(**15**) 2.396(5)
	Ch−Ge−Ch	(**17**) 92.54(6)	(**5**) 81.26(2)	(**15**) 84.75(1)
	Ge−Ch−C	(**17**) 128.03(13)	(**5**) 113.58(5)	(**15**) 108.8(5)
Sn	Sn−Ch	(**19**) 2.0472(17)	(**9**) 2.470(1)	(**16**) 2.594(3)
	Ch−Sn−Ch	(**19**) 92.18(6)	(**9**) 78.63(3)	(**16**) 78.60(3)
	Sn−Ch−C	(**19**) 129.25(15)	(**9**) 113.8(1)	(**16**) 112.1(3)
Pb	Pb−Ch	(**20**) 2.216(8)	(**12**) 2.5656(9)	
	Ch−Pb−Ch	(**20**) 99(1)	(**12**) 77.21(4)	
	Pb−Ch−C	(**20**) 127(2)	(**12**) 113.42(11)	

in the asymmetric unit has two tin sites, A and B, with 71/29% occupancy. The main difference in the two sites is the disparity of the S−Sn bond lengths. For site A, the S−Sn bond lengths are 2.4919(6) Å and 2.4114(6) Å, whereas for site B, the lengths are 2.3530(12) Å and 2.5235(12) Å. The Sn-centroid distances for site A are 3.160 Å (centroid 1) and 3.492 Å (centroid 2). For site B, the distances between the centroids are similar at 3.498 Å (centroid 1) and 3.151 Å (centroid 2). The shorter Sn-centroid distances in the mixed occupancy molecule are comparable to the Sn-centroid distances in the other molecule in the asymmetric unit at 3.126 and 3.155 Å.

A possible explanation of the two different tin sites in $Sn(SAr^{Pr^i_6})_2$ (**10**) (Figure 6) as observed by X-ray crystallography and Mössbauer spectroscopy (see below) is that at low temperatures the structures, which are related by the asymmetric b_2 vibration of the SnS_2 moiety, are close in energy and are stabilized by steric, dispersion, and packing forces. When the crystals are dissolved at ambient temperature, only one ^{119}Sn NMR signal is observed; indicating that the structures are indistinguishable by the slower time scale of the NMR technique, or that there is only one structure. Although this complex displays some of the characteristics of bond-stretch isomerism,[41] several attempts to model the two environments resulted in only one minimum on the potential energy surface corresponding to a symmetric S−Sn−S moiety.

^{29}Si, ^{77}Se, ^{119}Sn, and ^{207}Pb NMR Spectroscopy. The ^{29}Si spectrum of $Si(SAr^{Me_6})_2$ features a downfield singlet at δ = 285.5.[12] Signals for the bulkier silylenes $Si(SAr^{Pr^i_4})_2$ and $Si(SAr^{Pr^i_6})_2$ were located at similar chemical shifts but slightly upfield at δ = 270.4 and 270.9, respectively. The very similar shifts obtained for the silylenes show that the relatively small (≤6°) angular changes at silicon have a minor effect on the chemical shift of the thiolate derivatives.

The ^{119}Sn NMR spectra indicate a progressive downfield shift as the interligand angle decreases.[42] $Sn(SAr^{Me_6})_2$ has a signal at δ = 763.8, whereas $Sn(SAr^{Pr^i_4})_2$ and $Sn(SAr^{Pr^i_6})_2$ display signals δ = 814.8 and 827.4, respectively, and the signal of $Sn(SAr^{Pr^i_8})_2$ has the furthest downfield shift at δ = 919.4. The ^{119}Sn NMR chemical shifts of $Sn(SAr^{Pr^i_4})_2$ (δ = 814.8), $Sn(SeAr^{Pr^i_4})_2$ (δ = 1148.1), and the previously reported $Sn(OAr^{Pr^i_4})_2$ (δ = −289.7)[40] clearly illustrate the very large effects of the different chalcogenolate ligands. The trend is opposite of what one would expect based on σ-inductive effects. The more electropositive substituents decrease the HOMO−LUMO gap, and as a result, increase the paramagnetic deshielding which augments the applied field and causes a downfield chemical shift on the ^{119}Sn NMR signal.[43,44]

A comparison of the chemical shifts for stannylene dichalcogenolates with other two coordinate stannylenes shows their ^{119}Sn NMR signal to be downfield of stannylene diamides, such as $Sn\{N(SiMe_3)_2\}_2$ (δ = 746),[44] and upfield of dialkyl or diaryl stannylenes, such as $Sn\{CH(SiMe_3)_2\}_2$ (δ = 2328)[45] and $Sn(Ar^{Me_6})_2$ (δ = 1971).[46] The signals of $Sn(SAr^{Pr^i_8})_2$ and $Sn(SeAr^{Pr^i_4})_2$ are close to that observed for the diarylstannylene $Sn(Mes^*)_2$ (δ = 980) (Mes* = C_6H_2-2,4,6-Bu^t_3).[3]

The ^{207}Pb NMR spectra of the lead thiolates demonstrated only small shift differences upon varying the thiolate ligands (in comparison to the very wide dispersion range of ^{207}Pb NMR shifts in general).[47] Plumbylenes $Pb(SAr^{Pr^i_4})_2$, $Pb(SAr^{Pr^i_6})_2$, and $Pb(SAr^{Pr^i_8})_2$ have signals in the narrow range of 4283−4335 ppm. These are comparable to other monomeric plumbylenes, such as $Pb\{N(SiMe_3)_2\}_2$, which has a chemical shift at δ = 4916,[47] though they are much further downfield of that of the previously reported $Pb\{N(H)Ar^{Me_6}\}_2$ (δ = 2871).[10] The difference between these two amido plumbylenes is believed to be due to the interaction of flanking aryl rings of $Pb\{N(H)Ar^{Me_6}\}_2$ with the lead atom.

The ^{77}Se NMR spectra for $Ge(SeAr^{Pr^i_4})_2$ and $Sn(SeAr^{Pr^i_4})_2$ display signals that have a greater downfield shift for the germylene (δ = 657.5) in comparison to the stannylene analogue (δ = 526.9). The difference is likely due to an inductive effect since germanium is more electronegative than tin. The region of ^{77}Se NMR shifts for both metals is characteristic of organic selenides.[48] The $^1J_{SeSn}$ coupling observed in the ^{77}Se NMR spectrum of $Sn(SeAr^{Pr^i_4})_2$ is 516 Hz, which represents an average of the ^{119}Sn or ^{117}Sn couplings due to broad signals. This is similar to the $^1J_{SeSn}$ coupling observed in the triselenolato Sn(II) complex, $NaSn(SePh)_3$ ($^1J_{SeSn} \approx 400$ Hz) (no reported structure), which has a chemical shift (δ = 164) significantly upfield of **15** and **16**.[49] A weak signal corresponding to the diselenide, $(SeAr^{Pr^i_4})_2$, was also located at δ = 480.2. Chemical shifts for the ^{29}Si, ^{77}Se, ^{119}Sn, and ^{207}Pb NMR spectra are shown in Table 5.

^{119}Sn Mössbauer Spectroscopy. The isomer shifts of stannylenes $Sn(SAr^{Me_6})_2$ (**8**), $Sn(SAr^{Pr^i_4})_2$ (**9**), $Sn(SAr^{Pr^i_6})_2$ (**10**),

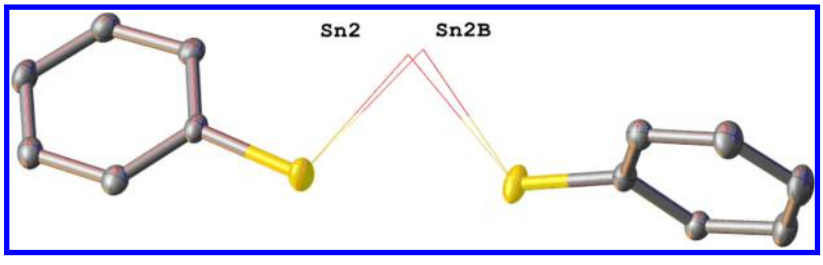

Figure 6. A drawing showing the two tin sites in the structure of $Sn(SAr^{Pr^i_6})_2$. For clarity, flanking arene groups are not shown.

dx.doi.org/10.1021/ja403802a | J. Am. Chem. Soc. XXXX, XXX, XXX−XXX

$Sn(SAr^{Pr^i_8})_2$ (**11**), $Sn(SeAr^{Pr^i_4})_2$ (**16**), and $Sn(OAr^{Pr^i_4})_2$ (**19**) all appear above 2.65 mm/sec^{-1}, so clearly all of these correspond to Sn(II).[50] For the stannylenes $Sn(SAr^{Pr^i_4})_2$ (**9**) and $Sn(SAr^{Pr^i_6})_2$ (**10**), two tin sites are present, in approximately a 2:1 ratio at 90 K (Figure 7). While the isomer shift difference between the two sites is relatively small, the quadrupolar splitting is significantly different. The two signals can be assigned to a change in the geometry of the tin sites leading to a large difference in the electric field gradient tensor at the metal site. As mentioned earlier, in the X-ray crystal structure, one of the two molecules of **10** at 90 K reveals two tin sites with occupancies of 71 and 29%. While this ratio does not match that seen in the Mössbauer effect (ME) spectra (is ca. 50% of the ratio), it does show that two tin sites with similar electronic but different geometric structures can coexist in the solid state. All of the ^{119}Sn ME data are summarized in Table 6, in which the hyperfine parameters (IS and QS) are those observed at 90 K. The IS values are reported with respect to a room temperature absorber spectrum of $BaSnO_3$. The data relating to the mean-square amplitude-of-vibration (msav) of the tin atoms in the various compounds are noteworthy. The msav is most readily expressed in terms of the parameter $F = -k^2 < x^2 > k^2$. This parameter can be evaluated from the ^{119}Sn ME data ($F_{X,T}$) as well as the $U_{i,j}$ values determined in the X-ray studies ($F_{X,T}$) all at temperatures T.[51] The ^{119}Sn ME F parameters were calculated from the temperature dependence of the logarithm of the

Table 5. ^{29}Si, ^{77}Se, ^{119}Sn, and ^{207}Pb Heteronuclear NMR Chemical Shifts for Tetrylene Dichalcogenolates

	δ: ^{29}Si	δ: ^{77}Se	δ: ^{119}Sn	δ: ^{207}Pb
(**1**) $Si(SAr^{Me_6})_2$	285.5			
(**2**) $Si(SAr^{Pr^i_4})_2$	270.4			
(**3**) $Si(SAr^{Pr^i_6})_2$	270.9			
(**8**) $Sn(SAr^{Me_6})_2$			763.8	
(**9**) $Sn(SAr^{Pr^i_4})_2$			814.8	
(**10**) $Sn(SAr^{Pr^i_6})_2$			827.4	
(**11**) $Sn(SAr^{Pr^i_8})_2$			919.4	
(**12**) $Pb(SAr^{Pr^i_4})_2$				4283
(**13**) $Pb(SAr^{Pr^i_6})_2$				4299
(**14**) $Pb(SAr^{Pr^i_8})_2$				4335
(**15**)$Ge(SeAr^{Pr^i_4})_2$		657.5		
(**16**)$Sn(SeAr^{Pr^i_4})_2$		526.9[a]	1148	
(**18**) $Sn(OAr^{Me_6})_2$			−344	
(**19**) $Sn(OAr^{Pr^i_4})_2$			−289.7	
(**20**) $Pb(OAr^{Pr^i_4})_2$				1070

[a] $^1J_{SeSn}$ = 516 Hz.

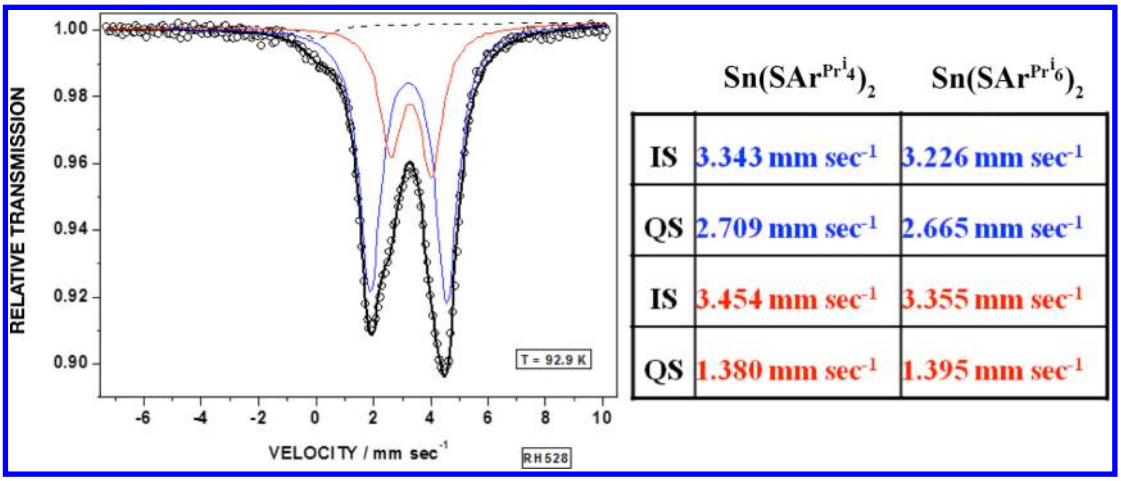

Figure 7. Mössbauer spectrum for $Sn(SAr^{Pr^i_4})_2$ (**9**) at 93 K, with tabular data for $Sn(SAr^{Pr^i_6})_2$ (**10**) also included. Two signals, in an almost identical ratio, are also observed for $Sn(SAr^{Pr^i_6})_2$. Only one tin site is observed for compounds $Sn(SAr^{Me_6})_2$ and $Sn(SAr^{Pr^i_8})_2$.

Table 6. Summary of the ^{119}Sn Mössbauer Effect Results cited in the Text[a]

	8	9	10	11	16	19	units
$IS_1(90)$	3.08(1)	3.34(1)	3.23(1)	3.34(1)	3.30(2)	3.15(1)	mm sec^{-1}
$QS_1(90)$	2.03(1)	2.71(1)	2.67(1)	2.60(1)	2.59(2)	2.10(1)	mm sec^{-1}
$IS_2(90)$		3.45(1)	3.36(1)				mm sec^{-1}
$QS_2(90)$		1.38(1)	1.40(1)				mm sec^{-1}
$-dIS_1/dT$		~indep	1.4(3)	~4.6(1)			mm sec^{-1}/K × 10^{-4}
$-dIS_2/dT$		~indep	~indep				mm sec^{-1}/K × 10^{-4}
$-dQS_1/dT$		~indep	3.4(3)	~8.(1)	2.2(4)		mm sec^{-1}/K × 10^{-4}
$-dQS_2/dT$		~indep	~indep				mm sec^{-1}/K × 10^{-4}
$-d \ln A_1/dT$	18.94(21)	25.13(16)	24.93(9)	17.55(41)	25.7(21)		K^{-1} × 10^{-3}
$-d \ln A_2/dT$		21.31(16)	19.53(9)				K^{-1} × 10^{-3}
$k_1^2 < x_{ave}^2 >_{M,88}$	1.68(8)	2.22(6)	2.19(5)	1.55(13)	2.27(9)	1.83(4)	
$k_1^2 < x_{ave}^2 >_{X,88}$	2.77(4)	2.99(6)	2.86(9)	2.63(2)	3.94(2)	2.79(1)	
$k_2^2 < x_{ave}^2 >_{M,88}$		1.89(6)					
ME/X-ray	0.61	0.74	0.76	0.59	0.58	0.66	

[a] The parenthetical values are the experimental errors in the last significant figure(s). The subscripts on the cited F parameters indicate M for the Mössbauer experiment results and X for the X-ray derived values.

dx.doi.org/10.1021/ja403802a | J. Am. Chem. Soc. XXXX, XXX, XXX−XXX

recoil-free fraction, which in turn, for an optically thin absorber, is equal to the temperature dependence of the logarithm of the area under the resonance curve. An assumption underlying this calculation is that $f \rightarrow 1$ as $T \rightarrow 0$, that is, that the zero point vibration is negligibly small compared to the msav in the cited temperature regime. The F_M values are smaller than the F_X values, the ratios ranging from 0.59 to 0.76. As has been shown in a number of recent studies involving iron and/or tin containing organometallics, the difference in the F factors is especially large when the metal atom (in this case Sn) is ligated to its nearest-neighbor environment by single σ, rather than multiple, bonds.[52] Such ligated atoms are sensitive to low-frequency rotational/librational motions, which are recorded in the X-ray determination but not in the ^{119}Sn Mössbauer data. This bonding feature is clearly evident in the structures of compound **8** and **11**.

The temperature dependence of the logarithm of the recoil-free fraction, $-\,\mathrm{d}\ln f/\mathrm{d}T$, for both **8** and **11**, *inter alia,* is well fitted by a linear regression, and thus the F parameter permits the evaluation of the root-mean-square amplitude-of-vibration (rmsav) of the tin atoms over the range $90 < T < 225$ K in the two structures. These rmsav values are summarized graphically in Figure 8, from which it is seen that the vibrational amplitudes in **8**

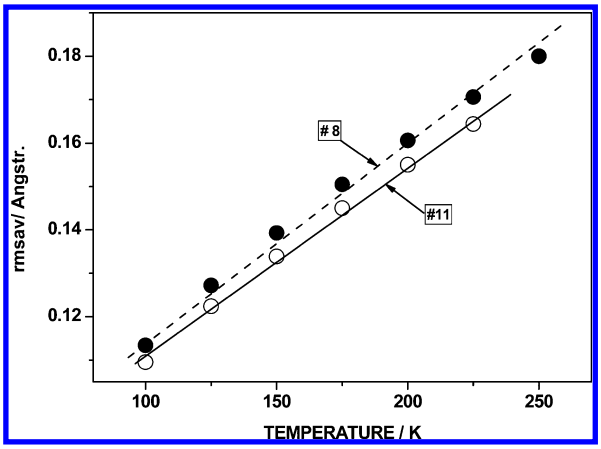

Figure 8. The rmsav of the Sn atoms in two of the compounds discussed in the text, calculated from the temperature-dependent ^{119}Sn Mössbauer data.

are somewhat larger than in **11**. Finally, it is worth noting that the temperature dependence of the recoil-free fraction in **9** and **16** are essentially identical, implying that replacing S (in **9**) by Se (in **16**) has little effect on the metal atom dynamics in the two compounds.

The X-ray crystal data for **10** suggest that the main difference in the two sites is the change of the S−Sn bond lengths. For the higher occupancy tin site, the two S−Sn bond lengths differ slightly at 2.4919(6) and 2.4114(6) Å, whereas in the low-occupancy site the lengths are 2.3530(12) and 2.5235(12) Å. The QS of 2.665 mm sec^{-1} appears to correlate with the more symmetric tin site with the smaller QS of 1.395 mm sec^{-1} corresponding with the asymmetric tin site.

Electronic Spectra. The electronic spectra of the divalent chalcogenolates (wavelengths and intensities are given in Table 7) are all characterized by transitions in the UV−vis and near-UV regions for the thiolates and selenolates and in the near UV for most of the aryloxo complexes.[12,33] We have reported recently that the experimental UV−vis spectrum of **1** can be interpreted with the help of TD-DFT calculations which showed

Table 7. Experimental Data for the Electronic Spectra of 1−16 and 20[a]

(**1**) $Si(SAr^{Me_6})_2$	(**2**) $Si(SAr^{Pr^i_4})_2$	(**3**) $Si(SAr^{Pr^i_6})_2$	(**4**) $Ge(SAr^{Me_6})_2$
382 (8300)	405 (3700)	411 (4400)	396 (3000)
318 (23 000)	318 (7400)	331 (7500)	276 (7700)
291 (20 000)	290 (11 200)	290 (10 500)	
269 (25 000)			
(**5**) $Ge(SAr^{Pr^i_4})_2$	(**6**) $Ge(SAr^{Pr^i_6})_2$	(**7**) $Ge(SAr^{Pr^i_8})_2$	(**8**) $Sn(SAr^{Me_6})_2$
410 (3100)	414 (3600)	430 (7200)	400 (1100)
330 (3600)	338 (3700)	362 (6100)	298 (5300)
278 (5600)	286 (4100)	282 (10 400)	292 (5300)
(**9**) $Sn(SAr^{Pr^i_4})_2$	(**10**) $Sn(SAr^{Pr^i_6})_2$	(**11**) $Sn(SAr^{Pr^i_8})_2$	(**12**) $Pb(SAr^{Pr^i_4})_2$
406 (1300)	414 (1400)	430 (2400)	422 (1300)
330 (1500)	342 (1700)	366 (2500)	354 (1100)
276 (3700)	276 (4900)	286 (4900)	292 (5800)
(**13**) $Pb(SAr^{Pr^i_6})_2$	(**14**) $Pb(SAr^{Pr^i_8})_2$	(**15**) $Ge(SeAr^{Pr^i_4})_2$	(**16**) $Sn(SeAr^{Pr^i_4})_2$
427 (1800)	446 (4200)	435 (7700)	434 (5800)
365 (1600)	372 (2500)	358 (9000)	368 (6900)
316 (2200)	292 (6600)	303 (8900)	305 (9500)
			296 (12 900)
(**20**) $Pb(OAr^{Pr^i_4})_2$			
370 (860)			
300 (3000)			
293 (3200)			

[a]Transition energy and intensities (in parentheses) given in nm and M^{-1} cm^{-1}.

the first low-energy transition at 382 nm to be a tetrylene n (HOMO) → tetrylene p (LUMO). However, as the orbital analysis in Figure 9 demonstrates, the exact bonding characteristics of the frontier orbitals in divalent chalcogenolates depend on the Ch−M−Ch bond angle, and no statements on the type of transitions observed in the electronic spectra of **2**−**16** can therefore be made based on the data available for **1**. The exact assignment of each experimental spectrum would require explicit TD-DFT calculations to be carried out for the specific molecule in question, which would be a very time-consuming undertaking. However, some general comments of trends in the experimental spectra can still be given.

As shown in Table 7, the lowest energy transition in **1**−**16** moves to longer wavelengths on descending group 14. Also, more electronegative group 16 substituents more effectively stabilize the tetrylene lone pair via an electron-withdrawing effect and increase the energy difference between the lone pair and the empty p orbital.[2] The energy of the transition also decreases with increasing ligand bulk. As the lowest energy transition is presumably of HOMO → LUMO type (however, it is not known if the structures in solution are the same as those in the crystal phase) in all systems studied, the above trends can be correlated to accompanying changes in the key structural parameters, that is, the Ch−M−Ch and M−Ch−C bond angles, which directly affect the energy of the HOMO (see Figure 9) and therefore the electronic spectrum.

The data from electronic spectra indicate that the heavier tetrylenes have a smaller HOMO−LUMO energy separation than their lighter congeners. Although similar trends have been observed previously,[6,10] this result is opposite of what is expected on the basis of a comparison with transient dialkyl or diaryl

dx.doi.org/10.1021/ja403802a | J. Am. Chem. Soc. XXXX, XXX, XXX−XXX

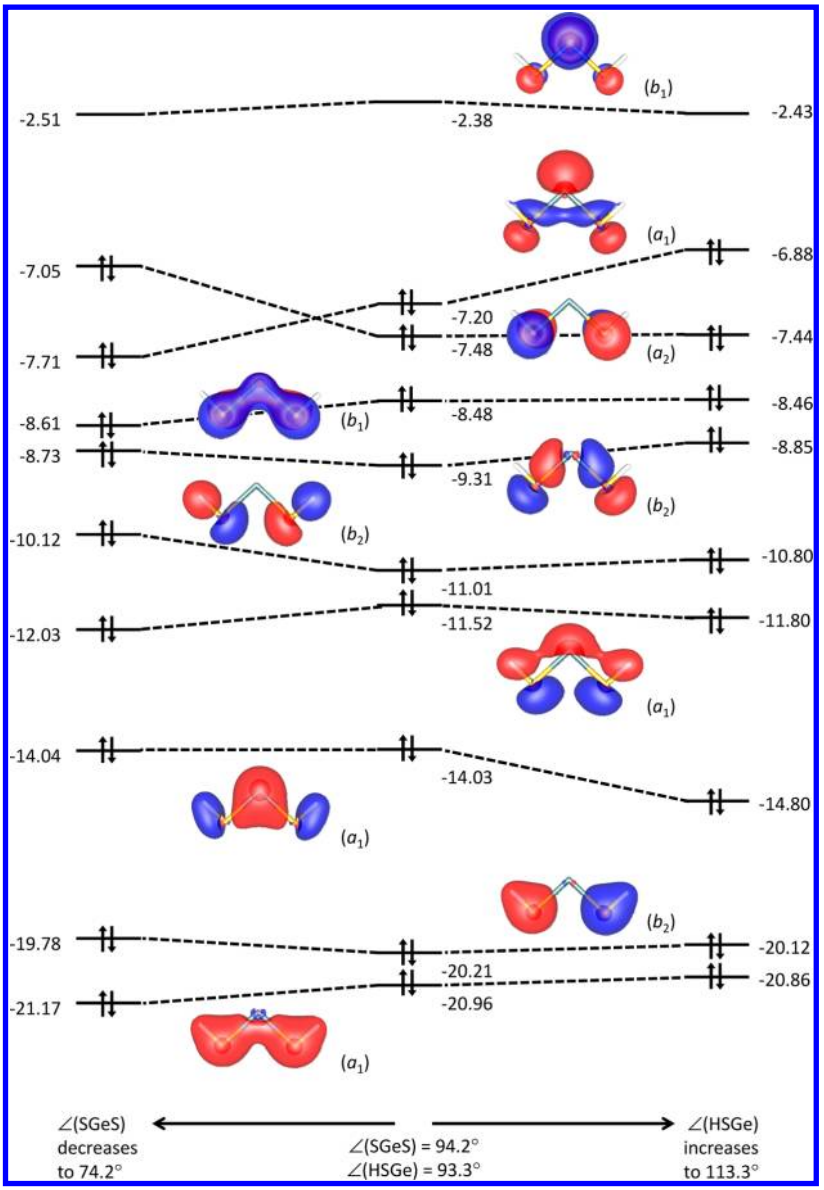

Figure 9. Valence Kohn−Sham MOs of H−S−Ge−S−H and their energies [eV].

species[6,53−56] or stable diaryl tetrylene complexes, such as $M(Ar^{Me_6})_2$ and $M(Ar^{Pr^i_4})_2$ (M = Ge−Pb).[6,57] These predict the transition energy should become greater descending the group based on the inert pair effect, where s electrons become progressively lower in energy upon descending the group.[58] The tetrylene lone pair orbital does in fact decrease in energy on descending group 14, but energy separation between energy levels may also decrease, due to the weakening of the bonds with increasing atomic number. Because of the acute bond angles, there are other orbitals that approach each other in energy in these systems (see Figure 9). Consequently, the low energy transitions observed in the experimental spectra of tin and lead derivatives may also originate from the π-type lone pairs on the chalcogen atoms and not from the tetrylene lone pair. Our recent analysis of the electronic spectrum of the silicon derivative **1** showed these transitions to reside only slightly higher in energy (around 60 nm in the experimental spectrum) compared to the transition with silylene n → p character.[12]

Orbital Analysis. The major factor producing the acute bond angles in tetrylenes **2**−**16**, as well as in other similar compounds, involves a combination of repulsive steric interactions and attractive dispersion forces between the bulky substituents across the axis that bisects the MCh_2 angle. For the terphenyls, the greatest repulsion comes from the *ortho*-substituents of the flanking arene rings on the lone pair side of the group 14 atom. The dispersion interactions occur both on the group 14 element lone pair side and the side of chalcogenolate ligands and may be visualized to best advantage in the illustration of the structure of **11** (Figure 2), where these *ortho*-isopropyl groups (and also the *para*-isopropyl groups) are brought into close approach. The interligand interactions cause the C−Ch−M bond angles to widen in order to relieve strain, which also cause the Ch−M−Ch angles to contract to sub-90° angles. There appears to be little direct interaction of the flanking arene rings with the metal based on heteronuclear NMR and ^{119}Sn Mössbauer spectroscopy and no significant distortions within the crystal structures.

To further investigate the structural trends in dichalocogenolate tetrylenes, a series of calculations was carried out using density functional theory (DFT). In particular, the role of electronic and steric effects in determining the Ch−M−Ch angle was analyzed by

dx.doi.org/10.1021/ja403802a | J. Am. Chem. Soc. XXXX, XXX, XXX−XXX

carrying out geometry optimizations for R−Ch−M−Ch−R, where M = Si, Ge, Sn, Pb; Ch = O, S, Se; and R = H, Ph, Tph, $Ar^{Pr^i_8}$ (Tph = C_6H_3-2,6-Ph_2). However, before discussing the results of these calculations, we begin by concentrating on an orbital-type analysis of bonding in dichalocogenolate tetrylenes and inspect the Kohn−Sham MOs of the parent molecular framework.

The valence MOs of the model species H−Ch−M−Ch−H have C_{2v} symmetry, and their relative energy levels are shown in Figure 9 (center) for Ch = S and M = Ge combination. The HOMO (a_1) corresponds to the tetrylene lone pair and the HOMO-1 (a_2) and HOMO-2 (b_1) are π-type bonding and nonbonding combinations of the p_z AOs at Ch and M; the LUMO (b_1) is the third π-type combination which is antibonding. By visual inspection of the orbitals, it becomes immediately evident that there is a net bonding contribution from two σ-type orbitals within the Ch−M−Ch moiety, which correspond to two single bonds. Furthermore, there is also a π-type bonding orbital, HOMO-2, but its contribution to Ch−M bonding is likely to be of less importance for systems with nonplanar R−Ch−M−Ch moieties (i.e., **1**−**14**) and, consequently, a lower symmetry C_2 point group.

Figure 9 also shows the changes in the valence MOs due to a 20° decrease in the Ch−M−Ch angle (left) or a 20° increase in the R−Ch−M angle (right) from the calculated lowest energy value near 94.2° and 93.3° respectively. What is most notable is that both perturbations induce major changes in the energies and shapes of only a few orbitals. Specifically, when the Ch−M−Ch angle decreases, the energy of the lone pair a_1 HOMO decreases as the orbital attains more Ch···Ch bonding character. This is supported by the ^{119}Sn Mössbauer spectra of stannylenes, **8**−**11**, where the isomer shift becomes more positive from **8** (3.08 mm sec^{-1}) to **12** (3.34 mm sec^{-1}) indicating an increase of electron density at the tin nucleus. At the same time, the energy of the π-type nonbonding orbital (a_2) increases as it gradually becomes more and more Ch···Ch antibonding. Consequently, at some point, these MOs will cross, and the nature of the HOMO will change. We note that with realistic substituents, the molecular point group is lowered to C_2 in which both HOMO and HOMO-1 transform according to the same irreducible representation, with the result that there will be an avoided crossing. In contrast to the above, widening the R−Ch−M angle in R−Ch−M−Ch−R increases the energy of the HOMO as it loses its Ch···Ch bonding character and becomes more M−Ch antibonding. Again, this change is counterbalanced by a decrease in the energy of one of the orbitals which attains more M−Ch bonding character upon increasing the R−Ch−M angle. However, in this case there is no associated change in the relative ordering of the orbitals as the two MOs are well separated in energy.

Figure 9 raises two important points. First, the relative ordering of the frontier MOs in dichalocogenolate tetrylenes is dependent on the key geometrical parameters which in turn depend heavily on the identity of the M and Ch atoms and the steric bulk of the aromatic substituent employed. Consequently, trends in, for example, the electronic spectra, are not expected to correlate with X-ray structural parameters in any straightforward manner (see above). Second, the potential energy surface of dichalocogenolate tetrylenes can, at least to some extent, adapt to changes in the geometrical parameters through changes in the nature of key orbital interactions. For example, the potential energy surface for the bonding of the Ch−M−Ch angle in parent dichalocogenolate tetrylenes is calculated to be particularly shallow, with energy increasing only a few kJ mol^{-1} per successive 1° decrease in the bond angle. This is in good agreement with the range of R−Ch−M−Ch−R systems that can be synthesized experimentally and the straightforward nature of the synthetic procedure used to obtain even the bulkiest derivatives (metathesis).

Optimized Structures. The results from geometry optimizations of R−Ch−M−Ch−R with different R groups (SI) show that electronic effects of the organic substituent have very little impact on the key geometrical parameters of the system. For example, the Ch−M−Ch angle hardly changes at all when comparing data for R = H systems to that of the corresponding R = Ph species. Accordingly, there is very little substituent induced change in the calculated atomic charge for the group 14 element. What is also notable from the calculated structures is that the Bent's rule is in general obeyed in both R = H and Ph series,[7,59] and the smallest Ch−M−Ch angles are found in bisphenoxides. This strongly suggests that the counterintuitive results obtained experimentally do not arise from electronic effects but instead predominantly from steric and dispersion factors. Furthermore, in all systems studied the Ch−M−Ch angle spans a relatively modest range from 89.6° to 96.9° with the largest values obtained when M = Si (most s−p hybridization) and the smallest when M = Sn and Pb (least s−p hybridization).

The bonding in dichalocogenolate tetrylenes does not change markedly from that described above even when using the parent terphenyl ligand (Tph = C_6H_3-2,6-Ph_2) as a substituent. The calculated Ch−M bond lengths change somewhat only in the case of the most crowded Ch = O derivatives but the differences are at most 0.05 Å. Also, the range of optimized Ch−M−Ch bond angles is only slightly narrower than that calculated for R = Ph species, from 87.4° to 93.5°, indicating very little changes in the electronic structure of the Ch−M−Ch moiety. Clearly the parent terphenyl ligand (Tph) is not sterically encumbering enough to alter the key bonding characteristics of these systems to any significant degree. This is also apparent from the calculated C−Ch−M bond angles which are between 95° and 100° for all sulfur and selenium derivatives and are significantly less than those observed experimentally. We therefore turned our attention to the analysis of the more crowded structures for which X-ray data allows direct comparison between theory and experiment.

The calculated key metrical parameters for the $R = Ar^{Pr^i_8}$ series are summarized in Table 8. A comparison with the available experimental data (Table 1) shows the two sets of numbers to be in reasonable agreement with each other: the calculated Ch-M bond lengths are accurate to less than 0.05 Å and the optimized Ch−M−Ch are only around 5° wider than those found experimentally. However, what is most notable is that the calculated structures reproduce the "inverse" of Bent's rule that has been observed experimentally—the widest Ch−M−Ch angles are found for Ch = O, around 100°, and the narrowest for Ch = Se, in which case angles close to 75° are seen. Consequently, for the bisphenoxide tetrylenes, there is too much steric repulsion, as well as interelectronic repulsion between the O-M bonding pairs, to permit acute interligand bond angles to occur. This is mainly due to their short C−O distances as compared to C−S and C−Se bonds in corresponding thiolato and selenolato derivatives. The calculations also accurately reproduce the increase in the R-Ch-M bond angle upon increasing the steric bulk of the substituent employed.

It would be reasonable to assume that the remaining discrepancies between the data in Tables 1 and 8 are attributable to packing effects generated by the large terphenyl substituents as these are not modeled in calculations. However, as has

dx.doi.org/10.1021/ja403802a | J. Am. Chem. Soc. XXXX, XXX, XXX−XXX

Table 8. Selected Bond Lengths [Å] and Angles [°] for Calculated Structures of Formulae $Ar^{Pr^i_8}$–Ch–M–Ch–$Ar^{Pr^i_8}$, where M = Si–Pb and Ch = O–Se

		PBE0/TZVP				disp. corr. PBE0/TZVP			
	Ch\M	Si	Ge	Sn	Pb	Si	Ge	Sn	Pb
r(ChM)	O	1.772	1.874	2.123	2.248	1.759	1.869	2.109	2.228
	S	2.210	2.322	2.553	2.647	2.203	2.315	2.539	2.631
	Se	2.354	2.442	2.663	2.751	2.348	2.435	2.649	2.736
∠MChM	O	99.1	96.2	96.0	97.3	96.4	93.0	92.3	93.0
	S	84.4	81.8	78.3	79.0	82.2	77.8	74.1	73.6
	Se	81.5	80.3	76.7	77.4	79.4	78.1	72.1	72.3
∠CChM	O	136.6	136.7	136.1	136.2	136.7	133.4	134.6	134.6
	S	117.2	117.6	117.9	118.1	116.4	117.6	119.0	119.8
	Se	115.5	115.2	115.2	115.5	114.6	114.0	117.8	117.5

recently been shown[60] for the quintuple bonded complex, $Ar^{Pr^i_4}CrCrAr^{Pr^i_4}$,[61] dispersion forces can play an important role as secondary bonding interactions capable of stabilizing compounds with exotic bonding environments[62] and bulky substituents. To this end, we tested the effect of empirical dispersion correction (Grimme's DFT-D3)[27] on the geometry optimization of the studied R = $Ar^{Pr^i_8}$ series (see Table 8). The results show that dispersion has the largest impact on the Ch–M–Ch bond angle which decreases by 2–5° throughout the series, therefore improving the agreement between theoretical and experimental structures. The Pb–S derivative, $Pb(SAr^{Pr^i_8})_2$ (**14**), makes an interesting exception to the above: calculations predict it to have a similar geometry to its lighter group 14 congeners, that is also seen with the less sterically crowded plumbylenes, $Pb(SAr^{Pr^i_4})_2$ (**12**) and $Pb(SAr^{Pr^i_6})_2$ (**13**), whereas the experimental structure of $Pb(SAr^{Pr^i_8})_2$ (**14**) shows a surprisingly wide S–Pb–S angle (80.07(2)°) accompanied by a significant twist in the relative orientation of the two terphenyl groups. However, the two S–Pb bond lengths are essentially equivalent in the experimental structure and comparable to the calculated values, indicating that the discrepancy in the bond angles could simply be a packing effect since there are four solvent molecules in the crystal structure of **14**, while there are none in those of **7**, **11**, or in the theoretically calculated $Si(SAr^{Pr^i_8})_2$.

The acute Ch–M–Ch bond angles in dichalocogenolate tetrylenes are in many cases accompanied by short intramolecular Ch···Ch distances[63] that are well below the sum of van der Waals radii for the respective elements (see Tables 1–3). This raises the important question of the chalcogen atoms sharing an orbital-type (covalent) bonding interaction between them. A visual inspection of the valence Kohn–Sham orbitals for H–S–Ge–S–H (Figure 9) shows that there is a net Ch···Ch bonding contribution from one MO which is that of the tetrylene lone pair.[64,65] As the Ch–M–Ch angle becomes more acute, the energy of this MO is lowered and the Ch···Ch interaction strengthened. However, as previously discussed, the change is accompanied with an increase in the energy of the π-type HOMO-1 which simultaneously acquires more Ch···Ch antibonding character. It is therefore not entirely surprising that an analysis of the theoretically determined total electron densities of dichalocogenolate tetrylenes with Bader's quantum theory of atoms in molecules (QTAIM)[66] failed to locate a bond critical point connecting the chalcogen centers in any of the model systems studied. Consequently, the short intramolecular Ch···Ch distances are mostly a result of geometrical constrains, augmented with dispersion forces as evidenced by a comparison of the two sets of theoretical results for the R = $Ar^{Pr^i_8}$ series.

It is interesting to note that the build-up of electron density in between the chalcogen atoms can be seen from the experimentally determined difference electron density maps. For example, examination of the electron density map for $Pb(SAr^{Pr^i_8})_2$ shows electron density centralized within the plane of the S–Pb–S angle (Figure 10). Additionally, the map of $Sn(SAr^{Me_6})_2$

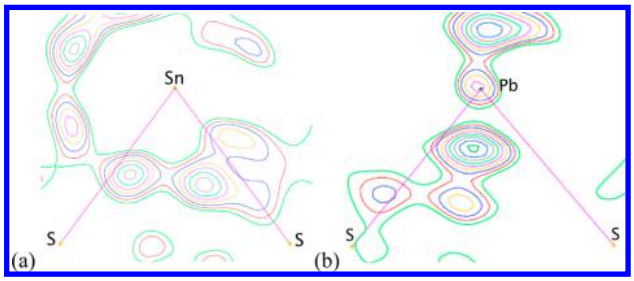

Figure 10. Difference electron density map of (a) $Sn(SAr^{Pr^i_8})_2$ (**11**) shows contours of electron density bisecting the two M–S bonds. (b) $Pb(SAr^{Pr^i_8})_2$ (**14**) shows a buildup of electron density within the S–Pb–S plane. Lines are shown connecting the sulfur and lead nuclei.

reveals no appreciable electron density in a centralized point within the S–Sn–S system. The difference map of the highly bent stannylene, $Sn(SAr^{Pr^i_8})_2$, reveals yet a different picture where one sees a large buildup of electron density bisecting the Sn–S bonds.

Finally, we note that an analysis[35b] of the structural distortions of tetravalent chalcogenolato group 14 element derivatives of formula $M(ChR)_4$ (M = C–Pb; Ch = O, S) has shown that the changes in the Ch–M–Ch angles can be rationalized in terms of the C–Ch–M–Ch–C conformations. The Ch–M–Ch angle increases as the number of eclipsed chalcogen lone pairs decreases (as indicated by the C–Ch–M–Ch angle). However, there is no analogous pattern in compounds **1**–**14**, where the number of eclipsed chalcogen lone-pairs (cf. C–S–M–S angles in Table 1) do not correlate well with substituent size.

CONCLUSIONS

(1) The principal forces leading to the sub-90° bond angles observed in the chalcogenolato tetrylenes are those of intramolecular steric repulsion and dispersion between the bulky substituents across the molecules.
(2) Dispersion forces stabilize the acute interligand angles.

dx.doi.org/10.1021/ja403802a | J. Am. Chem. Soc. XXXX, XXX, XXX–XXX

(3) Decreases in the bending angle below 90° for the heavier chalcogenolate derivatives require relatively small changes (ca. 1 kJ mol^{-1} deg^{-1}) down to Ch−M−Ch angles of ca. 70°.
(4) The size of the chalcogen has a large effect on the geometry of the tetrylenes. Because of the small radius of oxygen, there is significantly greater interligand and bond pair−bond pair repulsion that prevents closure of the interligand angle much below 90°. The size increase between oxygen (radius = 0.63 Å) and sulfur (1.03 Å) or selenium (1.16 Å) is large, so that bond pair−bond pair repulsion is diminished. This greatly reduces the amount of energy required to close the S(Se)−M−S(Se) angle below 90°. The wider M−O−C angles (ca. 10−20° wider than M−S−C angles) also reduce steric repulsion across the molecular axis on the tetrel lone pair side of the molecule which reduces the steric pressure to close the O−M−O angle. Additionally, electronegativity plays a minor role in determining the angles. The high electronegativity of oxygen promotes greater p character in its bonds relative to the more electropositive sulfur and selenium (which are still significantly more electronegative than the central metals) which favors an interligand angle closer to 90°.

■ ASSOCIATED CONTENT

Supporting Information

Experimental details for compounds **4**, **7**, **9**−**11**, **13**, **16**, **27**, **28**, and **30**−**35**; crystallographic information files, thermal ellipsoid plots, and tables of crystallographic data for **2**, **4**, **5**, **7**−**11**, **13**−**16**, **27**, **28**, and **30**−**35**; crystallographic data and files for the high residual value structures of **3** and **6**. ^{29}Si NMR spectra for silylenes **2** and **3**; ^{77}Se NMR spectra for **15** and **16**; ^{119}Sn NMR spectra for **8**−**11** and **16**; ^{207}Pb NMR spectra for **13** and **14**; ^{119}Sn Mössbauer spectrum for **19**; Plot of $k^2 < x_{ave}^2 >$ as a function of temperature for **19**; further discussion regarding the effect of ligand bulk on the synthesis of silylenes **1**-**3**; key structural parameters of calculated model systems and optimized structures (*xyz* data) of $Ar^{Pr^i_8}$−Ch−M−Ch−$Ar^{Pr^i_8}$ (M = Si−Pb; Ch = O−Se). This material is available free of charge via the Internet at http://pubs.acs.org.

■ AUTHOR INFORMATION

Corresponding Authors

pppower@ucdavis.edu; rolfe.herber@mail.huji.ac.il; heikki.tuononen@jyu.fi

Notes

The authors declare no competing financial interest.

■ ACKNOWLEDGMENTS

We are grateful to the U.S. National Science Foundation for funding this research (Grant CHE-09848417) and for the dual source X-ray diffractometer (Grant 0840444). We would also like to thank the Academy of Finland, the University of Jyväskylä, the Technology Industries of Finland Centennial Foundation for generous financial support. The authors are indebted to Prof. I. Nowik for fruitful discussions relating to the ME data reported here and Prof. K. C. Molloy for useful discussions regarding the conformations of **1**−**14**.

■ REFERENCES

(1) Power, P. P. *J. Organomet. Chem.* **2004**, *689*, 3904−3919.
(2) Fischer, R. C.; Power, P. P. *Chem. Rev.* **2010**, *110*, 3877−3923.
(3) For an example of large geometrical distortions due to steric effects, see: Yoshifuji, M.; Shima, M.; Inamoto, N.; Hirotsu, K.; Higuchi, T. *Angew. Chem., Int. Ed.* **1980**, *19*, 399−400.
(4) Hinchley, S. L.; Morrison, C. A.; Rankin, D. W. H.; Macdonald, C. L. B.; Wiacek, R. J.; Voigt, A.; Cowley, A. H.; Lappert, M. F.; Gundersen, G.; Clyburne, J. A. C.; Power, P. P. *J. Am. Chem. Soc.* **2001**, *123*, 9045−9053.
(5) Weidenbruch, W.; Schlaefke, J.; Schafer, A.; Peters, K.; von Schering, H.-G.; Marsmann, H. *Angew. Chem., Int. Ed.* **1994**, *33*, 1846−1848.
(6) (a) Lee, V. Y.; Sekiguchi, A. *Organometallic Compounds of Low-Coordinate Si, Ge, Sn and Pb: From Phantom Species to Stable Compounds*; John Wiley & Sons Ltd: Chichester, UK, 2010; 139−188., (b) Mizuhata, Y.; Sasamori, S.; Tokitoh, N. *Chem. Rev.* **2009**, *109*, 3479−3511. (c) Tokitoh, N.; Ando, W. *Reactive Intermediate Chemistry*; Moss, R. A.; Platz, M. S.; Jones, M., Jr., Eds.; Wiley: Hoboken, 2004, Chapter 14. (d) Asay, M.; Jones, C.; Driess, M. *Chem. Rev.* **2011**, *111*, 354−396.
(7) (a) Bent, H. *J. Chem. Educ.* **1960**, *37*, 616−624. (b) Bent, H. *Chem. Rev.* **1961**, *61*, 275−311.
(8) (a) Cetinkaya, B.; Gümrükcü, I.; Lappert, M. F.; Atwood, J. L.; Rogers, R. D.; Zaworotko, M. J. *J. Am. Chem. Soc.* **1980**, *102*, 2088−2089. (b) The lead analog was shown to be a monomer in the solid-state based on weak X-ray data, see: Lappert, M. F. *Main Group Metal. Chem.* **1994**, *17*, 183−207. (c) Weinert, C. S.; Fenwick, A. E.; Fanwick, P. E.; Rothwell, I. P. *Dalton Trans.* **2003**, 532−539.
(9) Hitchcock, P. B.; Lappert, M. F.; Samways, B. J.; Weinberg, E. L. *J. Chem. Soc., Chem. Commun.* **1983**, 1492−1494.
(10) Merrill, W. A.; Wright, R. J.; Stanciu, C. S.; Olmstead, M. M.; Power, P. P. *Inorg. Chem.* **2010**, *49*, 7097−7105.
(11) Rekken, B. D.; Brown, T. M.; Olmstead, M. M.; Fettinger, J. C.; Power, P. P. *Inorg. Chem.* **2013**, *52*, 3054−3062.
(12) Rekken, B. D.; Brown, T. M.; Fettinger, J. C.; Tuononen, H. M.; Power, P. P. *J. Am. Chem. Soc.* **2012**, *134*, 6504−6507.
(13) Protchenko, A. V.; Birjkumar, K. H.; Dange, D.; Schwarz, A. D.; Vidovic, D.; Jones, C.; Kaltsoyannis, N.; Mountford, P.; Aldridge, S. *J. Am. Chem. Soc.* **2012**, *134*, 6500−6503.
(14) (a) Gehrhus, B.; Lappert, M. F.; Heinicke, J.; Boese, R.; Blaser, D. *Chem. Commun.* **1995**, 1931−1932. (b) Ghadwal, R. S.; Roesky, H. W.; Propper, K.; Dittrich, B.; Klein, S.; Frenking, G. *Angew. Chemie. Int. Ed.* **2011**, *50*, 5374−5378. (c) Moser, D. F.; Guzei, I. A.; West, R. *Main Group Met. Chem.* **2001**, *24*, 811−812. (d) Zark, P.; Schäfer, A.; Mitra, A.; Hasse, D.; Saak, W.; West, R.; Müller, T. *J. Organomet. Chem.* **2010**, *695*, 398−408. (e) Becker, J. S.; Staples, R. J.; Gordon, R. G. *Cryst. Res. Technol.* **2004**, *39*, 85−88. (f) Gehrhus, B.; Hitchcock, P. B.; Lappert, M. F. *Z. Anorg. Allg. Chem.* **2005**, *631*, 1383−1386. (g) Kong, L.; Zhang, J.; Song, H.; Cui, C. *Dalton Trans.* **2009**, 5444−5446. (h) Mitra, A.; Brodovitch, J. −C.; Krempner, C.; Percival, P. W.; Vyas, P.; West, R. *Angew. Chem., Int. Ed.* **2010**, *49*, 2893−2895.
(15) (a) Rieke, R. D.; Hudnall, P. M. *J. Am. Chem. Soc.* **1972**, *94*, 7178−7179. (b) Rachonz, J.; Walborsky, H. M. *Tetrahedron Lett.* **1989**, *30*, 7345−7348.
(16) (a) Freeman, P. K.; Hutchinson, L. L. *J. Org. Chem.* **1983**, *48*, 879−881. (b) Bogdanovic, B. *Acc. Chem. Res.* **1988**, *21*, 261−267.
(17) (a) Ellison, J. J.; Ruhlandt-Senge, K.; Power, P. P. *Angew. Chem., Int. Ed. Engl.* **1994**, *33*, 1178−1180. (b) Sutton, A. D.; Fettinger, J. C.; Rekken, B. D.; Power, P. P. *Polyhedron* **2008**, *27*, 2337−2340. (c) Niemeyer, M.; Power, P. P. *Inorg. Chem.* **1996**, *35*, 7264−7272.
(18) Zhu, Z.; Fischer, R. C.; Ellis, B. D.; Rivard, E.; Merrill, W. A.; Olmstead, M. M.; Power, P. P.; Guo, J.-D.; Nagase, S.; Pu, L. *Chem.—Eur. J.* **2009**, *15*, 5263−5272.
(19) Ellison, J. J.; Ruhlandt-Senge, K.; Hope, H.; Power, P. P. *Inorg. Chem.* **1995**, *34*, 49−54.
(20) Sheldrick, G. M. *SHELXTL*, version 6.1; Siemens Analytical X-ray Instruments, Inc.; Madison, WI, 2002.
(21) Sheldrick, G. M. *SHELXS-97 and SHELXL-97*; Universität Göttingen; Göttingen, Germany, 1997.
(22) (a) Dolomanov, O. V.; Bourhis, L. J.; Gildea, R. J.; Howard, J. A. K.; Puschmann, H. *J. Appl. Crystallogr.* **2009**, *42*, 339−341. (b) Hardman, N. J.; Wright, R. J.; Phillips, A. D.; Power, P. P. *J. Am. Chem. Soc.* **2003**, *125*, 2667−2679.

(23) (a) Mansell, S. M.; Herber, R. H.; Nowik, I.; Ross, D. H.; Russell, C. A.; Wass, D. F. *Inorg. Chem.* **2011**, *50*, 2252−2263. (b) Glaberson, W. http://www.megadaq.com.
(24) (a) *TURBOMOLE V6.3 2011*; a development of the University of Karlsruhe and Forschungszentrum Karlsruhe GmbH (1989−2007); TURBOMOLE GmbH (since 2007): available from http://www.turbomole.com. (b) Laaksonen, L. *J. Mol. Graph.* **1992**, *10*, 33−34. (c) Bergman, D. L.; Laaksonen, L.; Laaksonen, A. *J. Mol. Graphics* **1997**, *15*, 301−306.
(25) (a) Perdew, J. P.; Burke, K.; Ernzerhof, M. *Phys. Rev. Lett.* **1996**, *77*, 3865−3868. (b) Perdew, J. P.; Burke, K.; Ernzerhof, M. *Phys. Rev. Lett.* **1997**, *78*, 1396−1401. (c) Perdew, J. P.; Ernzerhof, M.; Burke, K. *J. Chem. Phys.* **1996**, *105*, 9982−9985. (d) Adamo, C.; Barone, V. *J. Chem. Phys.* **1999**, *110*, 6158−6170.
(26) Schäfer, A.; Huber, C.; Ahlrichs, R. *J. Chem. Phys.* **1994**, *100*, 5829−5835.
(27) Grimme, S.; Ehrlich, S.; Goerigk, L. *J. Comput. Chem.* **2011**, *32*, 1456−1465.
(28) Baceiredo and coworkers had earlier used Mg powder to synthesize low-valent silicon species, see: Gau, D.; Kato, T.; Saffon-Merceron, N.; Cossio, F. P.; Baceiredo, A. *J. Am. Chem. Soc.* **2009**, *131*, 8762−8763.
(29) Jones and Aldridge proposed a lithium bromo silylenenoid intermediate in the synthesis of their acyclic silylene, see: Ref 13 and Han, J. S.; Sasamori, T.; Mizuhata, Y.; Tokitoh, N. *Chem.−Asian J.* **2012**, *7*, 298−300.
(30) Lim, Y. M.; Cho, H. M.; Lee, M. E.; Baick, K. K. *Organometallics* **2006**, *25*, 4960−4964.
(31) Dickie, D. A.; MacIntosh, I. S.; Ino, D. D.; He, Q.; Labeodan, O. A.; Jennings, M. C.; Schatte, G.; Walsby, C. J.; Clyburne, J. A. C. *Can. J. Chem.* **2008**, *86*, 20−31.
(32) Shaw, R. A.; Woods, M. *J. Chem. Soc. A* **1971**, 1569−1571.
(33) (a) Apeloig, Y.; Karni, M.; West, R.; Welsh, K. *J. Am. Chem. Soc.* **1994**, *116*, 9719−9729. (b) Apeloig, Y.; Karni, M. *J. Chem. Soc., Chem. Commun.* **1985**, 1048−1049. (c) Michalczyk, M. J.; Fink, M. J.; DeYoung, D. J.; Carlson, C. W.; Welsh, K. M.; West, R.; Michl, J. *Silicon, Germanium, Tin Lead Compd.* **1986**, *9*, 75−83.
(34) (a) Grumbine, S. D.; Tilley, T. D.; Arnold, F. P.; Rheingold, A. L. *J. Am. Chem. Soc.* **1993**, *115*, 7884−7885. (b) Jutzi, P.; Steiner, W.; König, E.; Huttner, G.; Frank, A.; Schubert, U. *Chem. Ber.* **1978**, *111*, 606−614.
(35) (a) Kersting, B.; Krebs, B. *Inorg. Chem.* **1994**, *33*, 3886−3892. (b) Barone, G.; Hibbert, T. G.; Mahon, M. F.; Molloy, K. C.; Parkin, I. P.; Price, L. S.; Silaghi-Dumitrescu, I. *Dalton Trans.* **2001**, 3435−3445.
(36) (a) Kano, N.; Tokitoh, N.; Okazaki, R. *Organometallics* **1997**, *16*, 4237−4239. (b) Tokitoh, N.; Kano, N.; Okazaki, R. *Phosphorus, Sulfur and Silicon.* **1999**, *153*, 333−334.
(37) Pyykkö, P.; Matsumi, S. *Chem. -Eur. J.* **2009**, *15*, 186−197.
(38) (a) Seligson, A. L.; Arnold, J. *J. Am. Chem. Soc.* **1993**, *115*, 8214−8220. (b) Driess, M.; Janoschek, R.; Pritzkow, H.; Rell, S.; Winkler, U. *Angew. Chem., Int. Ed. Engl.* **1995**, *34*, 1614−1616.
(39) (a) Vedeneyev, V. I.; Gurvich, L. V.; Kondrat'yev, V. N.; Medvedev, V. A.; Frankevich, Y. L. *Bond Energies, Ionization Potentials, and Electron Affinities*; St. Martin's Press: New York, 1962. (b) Weinert, C. S. *Main Group Met. Chem* **2007**, *30*, 93−100.
(40) Stanciu, C.; Richards, A. F.; Stender, M.; Olmstead, M. M.; Power, P. P. *Polyhedron* **2006**, *25*, 477−483.
(41) Parkin, G. *Acc. Chem. Res.* **1992**, *25*, 455−460.
(42) Kennedy, J. D.; McFarlane, W.; Pyne, G. S. *Bull. Soc. Chim. Belg.* **1975**, *84*, 289−298.
(43) Paramagnetic contribution to NMR shift, see: (a) Ramsey, N. F. *Phys. Rev.* **1950**, *78*, 699−703. (b) Müller, T. *J. Organomet. Chem.* **2003**, *686*, 251−256.
(44) Wrackmeyer, B. *Annu. Rep. NMR. Spectrosc.* **1985**, *16*, 73−186.
(45) Zilm, K. W.; Lawless, G. A.; Merrill, R. M.; Millar, J. M.; Webb, G. G. *J. Am. Chem. Soc.* **1987**, *109*, 7236−7237.
(46) Simons, R. S.; Pu, L.; Olmstead, M. M.; Power, P. P. *Organometallics* **1997**, *16*, 1920−1925.
(47) Wrackmeyer, B. *Annu. Rep. NMR Spectrosc.* **2002**, *47*, 1−37.
(48) (a) Christiaens, I.; Piette, J. L.; Laitem, L.; Baiwir, M.; Denoel, J.; Llabres, G. *Org. Magn. Reson.* **1976**, *8*, 354−356. (b) Tan, K. S.; Arnold, A. P.; Rabenstein, D. L. *Can. J. Chem.* **1988**, *66*, 54−60.
(49) Arsenault, J. J. I.; Dean, P. A. W. *Can. J. Chem.* **1983**, *61*, 1516−1523.
(50) (a) Flynn, P. A. In *Mössbauer Isomer Shifts*; Shenoy, G. K., Wagner, F.E., Eds.; North Holland Pub. Co.: Amsterdam, 1978, pp 595 ff; (b) see also the discussion in Mössbauer Spectroscopy: , Greenwood, N. N. Gibb, T. C., Chapman Hall Ltd: London, 1972, pp 375 ff. (c) Zuckerman, J. J. In *Chemical Mössbauer Spectroscopy*; Herber, R. H., Ed.; Plenum Press: New York, 1984, pp 271 ff.
(51) Guo, J.-Y.; Xi, H. -W.; Nowik, I.; Herber, R. H.; Li, Y.; Lim, K. H.; So, C.-W. *Inorg. Chem.* **2012**, *51*, 3996−4001 and references therein.
(52) (a) Herber, R. H.; Nowik, I. *Phosphorus, Sulfur and Silicon* **2011**, *186*, 1336−40. (b) Herber, R. H. *J. Orgonomet. Chem.* **2012**, *717*, 41−44.
(53) (a) Magnusson, E. *J. Am. Chem. Soc.* **1984**, *106*, 1177−1185. (b) Magnusson, E. *J. Am. Chem. Soc.* **1984**, *106*, 1185−1191.
(54) Vancik, H.; Raabe, G.; Michalczyk, M. J.; West, R.; Michl, J. *J. Am. Chem. Soc.* **1985**, *107*, 4097−4098.
(55) Sakurai, H.; Sakamoto, K.; Kira, M. *Chem. Lett.* **1984**, 1379−1382.
(56) (a) Becerra, R.; Gaspar, P. P.; Harrington, C. R.; Leigh, W. J.; Vargas-Baca, I.; Walsh, R.; Zhou, D. *J. Am. Chem. Soc.* **2005**, *127*, 17469−17478. (b) Moriseev, A. G.; Leigh, W. J. *J. Am. Chem. Soc.* **2006**, *128*, 14442−14443. (c) Moiseev, A. G.; Leigh, W. J. *Organometallics.* **2007**, *26*, 6268−6276.
(57) Spikes, G. H.; Peng, Y.; Fettinger, J. C.; Power, P. P. *Z. Anorg. Allg. Chem.* **2006**, *632*, 1005−1010.
(58) (a) Drago, R. S. *J. Phys. Chem.* **1958**, *62*, 353−357. (b) Pyykkö, P. *Chem. Rev.* **1988**, *88*, 563−594.
(59) (a) Reed, A. E.; Schleyer, P. v. R. *J. Am. Chem. Soc.* **1987**, *109*, 7362−7371. (b) Reed, A. E.; Schleyer, P.v.R. *J. Am. Chem. Soc.* **1990**, *112*, 1434−1445.
(60) Ndambuki, S.; Ziegler, T. *Inorg. Chem.* **2012**, *51*, 7794−7800.
(61) Nguyen, T.; Sutton, A. D.; Brynda, M.; Fettinger, J. C.; Long, G. J.; Power, P. P. *Science* **2005**, *310*, 844−847.
(62) Schreiner, P. R.; Chernish, L. V.; Gunchenko, P. A.; Tikonchuk, E. Y.; Haussman, H.; Serafin, M.; Schlecht, S.; Dahl, J. E. P.; Carlson, R. M. K.; Fokin, A. A. *Nature.* **2011**, *477*, 308−311.
(63) Bleiholder, C.; Werz, D. B.; Köppel, H.; Gleiter, R. *J. Am. Chem. Soc.* **2006**, *128*, 2666−2674.
(64) (a) Naruse, Y.; Inagaki, S. *Top. Curr. Chem.* **2009**, *289*, 265−291. (b) Inagaki, S.; Goto, N.; Yoshikawa, K. *J. Am. Chem. Soc.* **1991**, *113*, 7144−7146. (c) Inagaki, S.; Yoshikawa, K.; Hayano, Y. *J. Am. Chem. Soc.* **1993**, *115*, 3706−3709. (d) Dewar, M. J. S. *J. Am. Chem. Soc.* **1984**, *106*, 669−682. (e) Sakai, S.; Inagaki, S. *J. Am. Chem. Soc.* **1990**, *112*, 7961−7964.
(65) Recently, the S_2^{3-} radical, with a weak S···S interactions ascribing to ca. 0.5 bond order, was proposed for the S_2 moiety in the $[Cu_3S_2]^{3+}$ ion, see: (a) Berry, J. F. *Chem. −Eur. J.* **2010**, *16*, 2719−2724. (b) Sarangi, R.; Yang, L.; Winikoff, S. G.; Gagliardi, L.; Cramer, C. J.; Tolman, W. B.; Solomon, E. I. *J. Am. Chem. Soc.* **2011**, *133*, 17180−17191.
(66) (a) Bader, R. F. W. *Acc. Chem. Res.* **1985**, *18*, 9−15. (b) Bader, R. F. W.; Slee, T. S.; Cremer, D.; Kraka, E. *J. Am. Chem. Soc.* **1983**, *105*, 5061−5068.